R. & M. No. 3301

MINISTRY OF AVIATION

AERONAUTICAL RESEARCH COUNCIL
REPORTS AND MEMORANDA

The Use of a Deep Electrolytic Tank as a Lifting-Surface Calculator

By H. S. WARD, B.Sc.,
DEPARTMENT OF CIVIL ENGINEERING, UNIVERSITY OF BIRMINGHAM

LONDON: HER MAJESTY'S STATIONERY OFFICE
1963
PRICE: £1 0s. 0d. NET

The Use of a Deep Electrolytic Tank as a Lifting-Surface Calculator

By H. S. WARD, B.Sc.,

DEPARTMENT OF CIVIL ENGINEERING, UNIVERSITY OF BIRMINGHAM

*Reports and Memoranda No. 3301**

July, 1961

Summary.

An investigation of a deep electrolytic tank, applied as a lifting-surface calculator, has been made. The reasons for the initial choice of apparatus, and its subsequent behaviour are detailed.

The calculator was developed for use with the investigation of plane surfaces, plane control surfaces and a symmetrically cambered wing.

The results have been compared with existing theoretical and experimental work. As a consequence, it seems that the calculator could be put to a more general use.

1. *Introduction.*

There are many physical quantities, under steady conditions in a homogeneous medium where the flux is conservative, that satisfy Laplace's equation. Among these quantities are gravitational, electrostatic, electrical and magnetical potential and temperature.

The analogy between the electrical potential in a continuous conducting medium and potential-flow theory, resulting from linearising the equations of fluid motion has been known for many years. As a result, over the past thirty years, the method has been applied to solve a large range of aerodynamic problems, Malavard[1] gives a comprehensive bibliography of work utilising the analogy, spanning the years from 1845 to 1949.

This report deals with one aspect only of the possible applications of the electrolytic tank, namely the lifting-surface calculator. The idea springs from lifting-surface theory which enables the flow parameters round a finite wing to be calculated. Several methods have already been developed utilising this theory (Refs. 2, 3, 4, 5, 6, 7, 8).

An electrolytic tank was chosen for the experiments because, as found by previous investigators, the apparatus presented fewer practical difficulties than encountered with other methods and because of its adaptability for solving a wide range of problems.

The object of the present investigation was, first of all, to make a detailed examination of various factors which might affect the operation of the tank and secondly, to carry out a programme of tests with a view to a more extensive use of electrolytic-tank analogies.

* Previously issued as A.R.C. 22,974.

2. *Theory of The Lifting-Surface Calculator.*

2.1. *Elements of Aerodynamic Theory.*

2.1.1. *Field equations.*—Consider a region of space containing a fluid of density $\rho(x, y, z, t)$ and a volume v, inside an arbitrary closed surface S, located in this region. Suppose $Q(t)$ be the mass of fluid inside the volume v at any instant.
Then,

$$Q(t) = \iiint_v \rho dv . \tag{1}$$

Let u denote the velocity of a typical particle of the fluid, then the principle of the conservation of mass implies that the rate of increase of the mass of fluid in v becomes,

$$\frac{dQ}{dt} = -\iint_S (\rho\bar{u}) d\bar{S} . \tag{2}$$

Differentiating (1) gives:

$$\frac{dQ}{dt} = \iiint_v \frac{\partial \rho}{\partial t} dv . \tag{3}$$

By Gauss's theorem (2) becomes:

$$\iint_S \rho\bar{u} d\bar{S} = \iiint_v \nabla\rho\bar{u} dv . \tag{4}$$

Combining (4), (3) and (2) gives equation (5);

$$\iiint_v \left[\frac{\partial \rho}{\partial t} + \nabla\rho\bar{u}\right] dv = 0 . \tag{5}$$

Since the integrand is assumed continuous and v is arbitrary,

$$\frac{\partial \rho}{\partial t} + \nabla\rho\bar{u} = 0 . \tag{6}$$

This is the equation of continuity.

If irrotational flow is assumed, then

$$\nabla \times \bar{u} = 0 . \tag{7}$$

As a result of (7), there exists a scalar function Φ, such that

$$u = \nabla\Phi , \tag{8}$$

where Φ is the velocity potential.
If incompressibility is also imposed on the flow, then

$$\frac{\partial \rho}{\partial t} = \rho\nabla\bar{u} = 0 . \tag{9}$$

Equations (8) and (9) give

$$\nabla \times \nabla\Phi = \nabla^2\Phi = 0 . \tag{10}$$

The case of compressible flow can be reduced to the form of equation (10), if small perturbations of a steady flow occur.

A few of the conditions that permit the linearisation of the equations of motion to take place are:

(*a*) Lifting surface is an infinitely thin plate.

(*b*) Camber of surface is small.

(*c*) Surface has small angle of incidence.

(*d*) Vortex sheet remains in plane of lifting surface.

(*e*) Undisturbed flow is a uniform steady stream.

The small-perturbation theory allows a linear-perturbation potential to be introduced such that

$$\Phi = Ux + \phi(x, y, z). \tag{11}$$

The flow described by equation (11) is very nearly parallel to the x axis, the velocity of the undisturbed flow in the x direction being U.

The linearised equations of sound propagation through a body of gas, when the flow is steady, the Prandtl-Glauert equations, are

$$p - p_\infty = -\rho_\infty U \frac{\partial \phi}{\partial x}; \tag{12}$$

$$\left(1 - \frac{U^2}{a_\infty{}^2}\right) \frac{\partial^2 \phi}{\partial x^2} + \frac{\partial^2 \phi}{\partial y^2} + \frac{\partial^2 \phi}{\partial z^2} = 0; \tag{13}$$

$a_\infty{}^2$ denotes the square of the speed of sound in the undisturbed gas.

p_∞ and ρ_∞ denote the pressure and density respectively of the unperturbed gas.

Equation (13) may be transformed into the form of (10), providing the flow is not transonic or supersonic, by the following affine transformation.

$$\begin{aligned} X &= x(1 - M^2)^{-1/2}; \\ Y &= y; \\ Z &= z. \end{aligned} \tag{14}$$

Thus the solution of an incompressible subsonic-flow problem can be adapted to solve a compressible problem with the surface distorted according to equations (14).

Finally both incompressible and subsonic compressible flows which are irrotational may be represented by the equation,

$$\nabla^2 \Phi = 0. \tag{15}$$

2.1.2. *Boundary conditions.*—The velocity potential Φ has been expressed in (11) as

$$\Phi(x, y, z) = Ux + \phi(x, y, z);$$

where ϕ is the perturbation potential, due to the presence of the lifting surface in the plane $z = 0$, on a stream with an unperturbed velocity U in the x direction.

The boundary conditions to be imposed on ϕ are

(*a*) $\phi \to 0$ at distances remote from the lifting surface. (16)

(*b*) $\dfrac{\partial \phi}{\partial x} = 0$ in the wake region. (17)

(*c*) $\phi_{TE} = \phi_w$. (18)

Equation (18) expresses the Kutta-Joukowsky condition. TE refers to the trailing edge, and W to the wake.

Finally the condition that the flow should be tangential to the lifting surface whose equation is $z = F(x, y)$ may be written as

$$\bar{F} \times \bar{u} = 0, \tag{19}$$

which becomes

$$U \frac{\partial F}{\partial x} - \frac{\partial \phi}{\partial z} = 0, \tag{20}$$

when terms higher than the second order are ignored.

Further functional relationships of ϕ are:

(a) ϕ is an odd function of z. (21)

(b) $\frac{\partial \phi}{\partial x}, \frac{\partial \phi}{\partial y}$ are odd functions of z. (22)

2.1.3. *Aerodynamic quantities.*—From linearised potential theory we obtain:

$$p - p_\infty = - \rho U \frac{\partial \phi}{\partial x}; \tag{23}$$

p_∞ is the free-stream pressure, p is the pressure at any point, and ρ the corresponding density.

The lift of a two-dimensional wing per unit width is given by

$$L = \rho U \Gamma; \tag{24}$$

where Γ is the circulation about the body.

The following parameters may be obtained from the known velocity-potential distribution, about a finite wing surface.

Section lift, $l(\eta)$

$$l(\eta) = - 2\rho U \phi(\eta_{\mathrm{TE}}) d\eta. \tag{25}$$

$\eta = y/b$, b being the semi-span of the surface. $\phi(\eta_{\mathrm{TE}})$ corresponds to the circulation of a two-dimensional wing.

Total lift, L

$$L = - 2\rho U b \int_{-1}^{+1} \phi(\eta_{\mathrm{TE}})\, d\eta. \tag{26}$$

Section pitching moment about the y axis, $m(\eta)$

$$m(\eta) = 2\rho U c \int_{\mathrm{LE}}^{\mathrm{TE}} \frac{\partial \phi}{\partial \xi} \xi\, d\xi. \tag{27}$$

LE is the leading edge, $\xi = x/c$ and c is the local chord.

Total pitching moment M

$$M = 2\rho U b \int_{-1}^{+1} d\eta \int_{\mathrm{LE}}^{\mathrm{TE}} c \frac{\partial \phi}{\partial \xi} \xi\, d\xi. \tag{28}$$

Section centre of pressure $\chi(\eta)$

$$\chi(\eta) = c\xi_{\mathrm{TE}} - c \int_{\mathrm{LE}}^{\mathrm{TE}} \frac{\phi d\xi}{\phi(\eta_{\mathrm{TE}})}. \tag{29}$$

Total centre of pressure χ

$$\chi = \frac{\int_{-1}^{+1} \left\{ c \left(\xi_{\mathrm{TE}} \phi_{\mathrm{TE}} - \int_{\mathrm{LE}}^{\mathrm{TE}} \phi d\xi \right) \right\} d\eta}{\int_{-1}^{+1} \phi_{\mathrm{TE}} d\eta}. \tag{30}$$

2.2. *Elements of Electric-Field Theory.*

2.2.1. *Field Equations.*—In a three-dimensional conducting body within which the flux is conservative, the electrical potential satisfies

$$\nabla(\sigma\nabla V) = 0\,; \tag{31}$$

where σ is the conductivity of the medium and V is the electric potential.

If the medium is now assumed to be isotropic, equation (31) becomes

$$\sigma\nabla \times \nabla V = \sigma\nabla^2 V = 0\,. \tag{32}$$

Equations (15) and (32) show the analogy between the Aerodynamic and Electrical-field equations.

2.2.2. *Boundary conditions.*—Two analogies have been used during this work which involve different boundary conditions in the electrical field for the same aerodynamic condition. These differences will be discussed in detail in the following sections.

The electrical boundary conditions common to both analogies are given here.

If the planform being investigated is symmetrical with respect to the plane $z0x$. (Figure 1) then as a result of equations (21) and (22) the field may be reduced to the region *abcdefgh* within the conducting medium (Figure 2).

Equation (17) indicates that along lines where y is constant, in the wake, there must be a constant potential.

Equation (18) shows that for smooth outflow at the trailing edge, the potential there must equal that in the wake immediately behind it.

The models used and the methods of applying the conditions described above are detailed in the following sections.

3. *The Analogies.*

The two analogies employed here to solve the lifting-surface problem have been called the direct and transverse analogies.

3.1. *The Direct Analogy.*

This analogy depends on the identity between the equations governing the electrical potential distribution in a conductor in which current is flowing, and the linearised equations of fluid motion.

Since the perturbation potential ϕ satisfies Laplace's equation it can be put in a non-dimensional form,

$$\frac{\phi}{Uc} = mV, \tag{33}$$

where m is some constant.

The boundary conditions to be applied on the plane occupied by the wing and its wake are given by equations (17), (18) and (20).

The representation of the wing-wake in the electrolytic tank may be understood by reference to Figure 3. Section 4.6 is devoted to a more detailed description of model construction and model factors which influence the experimental results.

Equation (17) represents the condition that no accelerated flow occurs in the wake along lines where y is constant. This is represented in the electrolytic tank by applying a constant potential to such lines. The wake region of the model was divided up into a number of parallel strips bound by

lines of constant y. Alternate strips were made up of conducting and insulating zones respectively. Thus a stepwise variation of potential across the wake could be imposed. The potential to which any conducting region was to be raised was in the first place indeterminate, and dependent upon the Kutta condition of smooth outflow at the trailing edge. Equation (17) was satisfied when

$$\Delta V = 0. \tag{34}$$

The Kutta-Joukowsky requirement means there must be no acceleration of flow from the trailing edge in a direction parallel to the main-stream flow. This may be achieved in the tank by equating the potential at the trailing-edge station to that of its corresponding wake strip, thus,

$$V_{\mathrm{TE}} = V_W. \tag{35}$$

In order that the flow should be tangential to the lifting-surface equation (20) must be satisfied over the region. Using equation (33) this condition becomes,

$$U \frac{\partial F}{\partial x} = mUc \frac{\partial V}{\partial z}. \tag{36}$$

Now the current intensity di crossing a surface element ds of an electrolyte is given by Ohm's Law as

$$\frac{di}{ds} = -\sigma \frac{dV}{dn}, \tag{37}$$

where n is the surface normal to ds.

Combining equations (36) and (37) the boundary condition to be applied over the wing region becomes

$$\frac{di}{ds} = -\sigma U \frac{\partial F}{\partial x} \times \frac{1}{mUc}. \tag{38}$$

Therefore, in the electrolytic tank an electrical current intensity, proportional to the inclination of the lifting surface to the free stream, is applied to represent tangential flow over the wing. The region of the model representing the wing was divided up into zones of area ds. Each area was a small conducting electrode isolated on all sides by insulating bands. As a result a stepwise variation of potential could be imposed on the wing surface.

The value of $\partial F/\partial x$ at the centre of these electrodes, when known, allows the magnitude of the current according to equation (38) to be calculated. This intensity is then fed into the electrode. The application of the current creates a potential distribution which is proportional to the velocity potential of the analogous fluid-flow problem.

The remaining boundary conditions to be discussed are those applied at the tank walls and the free surface of the electrolyte. All the problems dealt with in this work were symmetrical with respect to the plane $z0x$. This meant that no potential gradient arises on this plane. Zero gradient occurs in the electrolytic tank when the region is an insulator.

Equation (16) is interpreted in the tank by making the remaining tank walls insulators and keeping the water surface outside the wing-wake region at constant potential.

A diagram of the circuit used in the direct analogy is shown in Figure 4. The circuit arrangement had to achieve the following conditions.

(*a*) The free surface of the water outside the wing-wake area to be at a constant potential.

(*b*) A current intensity previously calculated to be fed into each electrode area of the wing.

(*c*) The potential in the wake strips to be adjusted until they equalled those at the corresponding trailing-edge station.

(*d*) A device enabling the potential distribution, resulting from the application of the conditions above, to be measured.

The first requirement was attained by placing a large electrode over the region and connecting it to the earth terminal of the alternating voltage supply.

The boundary condition on the wing was established by using large resistances to supply the required current. The use of large resistances considerably simplifies this condition and the method is dealt with in more detail in Section 5.10. Briefly the use of these large resistances keeps the tank potentials at a small percentage of the applied potential (Figure 5). The current flowing, then is

$$i \simeq \frac{V}{R_L}, \tag{39}$$

and so

$$\frac{V}{R_L} \simeq -\sigma ds \frac{\partial F}{\partial x} \frac{1}{mc}. \tag{40}$$

As a result of the above equations, a resistance can be chosen for each station where $\partial F/\partial x$ is known and the tangential-flow boundary condition is approximately satisfied. It is convenient at this point to indicate that the inverse problem may also be solved by this circuit. Thus if it was necessary to design a wing with a given pressure distribution over its surface, in the analogue set-up the current flowing through the resistances would be the unknown quantity.

The Kutta-Joukowsky condition was applied by the use of an auxiliary probe circuit (Figure 6), described in Section 4.5. Any potential difference between the wing and its wake was shown on a cathode-ray-oscilloscope screen. The wake potential was then varied by the wake potentiometers (Figure 4) until this difference was zero. This process was carried out for each of the spanwise trailing-edge positions. Inevitably the adjustment of one station affected those close to it but the process converged rapidly.

The potential distribution was taken by comparing the potential to be measured with that from a decade box placed across the supply. The features of this part of the apparatus are discussed more fully in Section 4.5.

3.2. *The Transverse Analogy.*

This method was originated and developed by Duquenne.[9] It is applicable only to plane lifting surfaces at an inclination α to the free stream.

Using the transverse analogy and making the substitution

$$\frac{\phi}{Uc\alpha} + \frac{z}{c} = mV, \tag{41}$$

certain new boundary conditions occur in the electrolytic-tank field.

Equation (41) modifies the condition applied on the wing surface. Combining equations (20), (38) and (41) and remembering that $(\partial F/\partial x) = -\alpha$ the current intensity to be applied on the wing is

$$\frac{di}{dS} = 0. \tag{42}$$

This means that the wing surface must be made an insulating sheet. The boundary conditions expressed by equations (17) and (18) are achieved as in the previous analogy. Figure 7 shows the form of model used in this analogy.

Equation (16) shows that as z increases ϕ decreases. Thus at a large depth h in the electrolytic tank

$$\frac{h}{c} = mV; \tag{43}$$

where V is the potential difference between the top and bottom surfaces of the tank. This means that a lower electrode must be placed on the tank floor.

The remaining tank-wall and water-surface conditions are as described for the direct analogy.

The circuit diagram is shown in Figure 8. The main differences between the two analogies are as follows:

(*a*) The wing surface of the model in the transverse analogy is an insulation sheet, whereas in the direct analogy it is a conducting area.

(*b*) In the transverse analogy a potential difference is applied between the top and bottom of the tank, but in the direct analogy the bottom electrode is not used.

The magnitude of the measured voltages are always greater in the transverse analogy and this explains the presence of the capacitor in the circuit, the function of which will be described later.

4. *Apparatus.*

The initial considerations and final choice of apparatus will be described in the following sections. The main items of equipment required to realise the analogies were:

(*a*) A continuous, homogeneous, conducting medium.

(*b*) A convenient model representation of the wing to be studied.

(*c*) A suitable power supply.

(*d*) Some means of voltage measurement.

(*e*) Arrangements for applying the remaining conditions discussed in the previous sections.

4.1. *The Electrolyte.*

Although it is possible to work with solids as the conducting medium, there are inherent difficulties associated with the method, such as the insulation of the region from external disturbances and the manufacture of such a solid. References to this sort of work have been given by Karplus.[10]

The value of an electrolyte depends on the degree to which it possesses the following properties:

(*a*) No electrical reactance.

(*b*) Uniform resistivity.

(*c*) The resistivity is large compared to that of the electrodes, and small compared to that of the input resistance of the sensing device.

(*d*) The resistivity is linear over the operating voltage range.

(*e*) It must be chemically inert.

(*f*) The surface-tension effects at the boundaries and probe should be small.

A detailed investigation of different electrode-electrolyte combinations was carried out by Einstein[11] to see how far they deviated from the ideals expressed above.

The results of Einstein's work showed that tap water was suitable, providing the excitation was an alternating voltage of relatively high frequency, to overcome polarisation effects at the electrodes.

With the aforementioned factors in mind, Birmingham tap water was chosen as the electrolyte and has been found satisfactory in most respects. The water is carried from the Elan Valley *via* an aqueduct to the Frankley Works in Birmingham. Here the water is treated, some typical values for ph and hardness are 7·7 and 20 p.p.m. respectively.

During the initial stages of the work an experiment was conducted with Staffordshire water, and gave rise to an interesting result discussed in Section 5.2. The corresponding figures for the ph value and hardness were 7·3 and 342 p.p.m.

4.2. *The Tank.*

The sides of an electrolytic tank should be smooth, watertight and good insulators. Wood is often used but must be varnished or otherwise treated to prevent swelling. Slate was chosen, therefore, on account of its insulation properties, impermeability and machineability.

The tank when constructed was eighty inches long, forty inches wide and thirty-two inches deep.

The sides of the tank were made up of single slabs of slate one and a half inches thick. Grooves were machined at the end of the slabs so that the sides could be slotted and bolted together. All joints were sealed with a bituminous plastic material.

Finally the tank was carefully sited on a levelled six inch bed of concrete on top of which was laid a sheet of Perspex a quarter of an inch thick.

4.3. *The Electrodes.*

Both the analogies used here assume that the aerofoil perturbs a steady uniform stream. Therefore, in each case, the area in the plane $z = 0$ outside the wing-wake region, has to be at a constant potential (Figures 3 and 8). In the electrolytic tank this plane is represented by the upper electrode. A cut had to be made in the electrode so the model representing the wing-wake system could be placed here (Figure 9).

The upper electrode rests on the tank walls, being supported by flat-plate brackets placed around its periphery; adjusting screws in these brackets allowed the electrode to be levelled. Because of its comparatively large span the electrode was made half an inch thick.

No electrode is required on the tank bottom for the direct analogy but one must be employed in the transverse analogy, to produce a potential gradient across the tank. As this electrode rests on the tank floor it can be made thinner than the upper electrode. Four circular threaded blocks were screwed on to this plate to facilitate its removal from the tank.

The electrode material should present a smooth well defined surface, which can be machined easily. Because of the merit given by Einstein[11] to different electrodes, three sets were manufactured for this work. The materials used were brass, stainless steel, and an aluminium alloy.

4.4. *Excitation.*

The electrical excitation of conductive-liquid systems is generally by an alternating-voltage supply. A steady voltage may be employed if it is great enough to overcome polarisation effects, but the potential field is still distorted in the region of high resistivity near to the electrode. Furthermore, permanent damage can occur to the electrodes as a result of electro-chemical reactions.

Einstein showed that as the frequency of the alternating voltage was increased so the surface-impedance effect decreased (Figure 10). Polarisation was also minimised by increasing the frequency

of excitation. Unfortunately, as the operating frequency is increased stray out-of-phase voltages become more pronounced. As a result of these factors it is necessary to investigate the optimum frequency of operation for each experimental arrangement used in the tank.

The alternating voltage supply chosen consisted of an audio-frequency generator covering 0 to 16000 c/s, and an a.c. amplifier.

The magnitude of the sinusoidal excitation was adjustable so that large current densities could be avoided. This precaution is necessary to prevent heating of the liquid, and certain non-linear effects experienced at electrodes by previous workers.

Sander[12] employed a square-wave voltage supply, and was able to eliminate all out-of-phase voltages. The method used during the development of this calculator did not completely eliminate the out-of-phase voltages but it was possible to measure them, and to reduce them to a satisfactory level.

4.5. *Voltage Measurement.*

There are two separate parts to the voltage measuring circuit, the probe and a null-indicator circuit.

4.5.1. *The probe.*—The insertion of a probe into an electric-potential field will inevitably distort the field. It was therefore essential to try to minimise this distortion if reasonable accuracy was to be obtained.

Burfoot[13] has produced a theoretical approach to the design of probes, of optimum shape and size. He showed that a rod-like shaped probe was more preferable than those of a disc or sphere-like shape.

Probe arrangements as shown in Figures 11 and 12 have proved satisfactory in practice, the main reason for their choice being cheapness and simplicity of construction.

4.5.2. *The null-indicator circuit.*—The null-indicator circuit had to pick up any voltage within the potential field, and compare it with some standard voltage.

Since a.c. excitation was used, a true null point could only be obtained when the amplitude and phase of the probe and standard signal coincided. As previously indicated, out-of-phase voltages arise in the tank and it was necessary to arrange this part of the circuit to minimise their effect.

There were a number of ways open to reduce these stray field effects, among them careful shielding of the probe, Wagner earth system and cathode followers. References 14 and 15 give details of the practical application of the last two methods.

The Wagner earth was thought to be rather cumbersome for the operations involved in the calculator, and on this score was abandoned. Cathode followers were not employed at this stage, as they were a piece of electronic equipment which require careful development for application to electrolytic-tank work and might have delayed the initial work described here.

The final choice of circuit is shown in diagrammatic form in Figure 13. The isolating transformer was contained in a metal shield to eliminate stray field effects. This type of transformer was essential if a sharp balance was to be obtained. The standard voltage was obtained by placing a non-inductively wound resistance box of 10,000 ohms, across the maximum voltage used during any experiment. The null indicator employed was a cathode-ray oscilloscope.

The probe and standard signal were applied to the vertical plates of the cathode-ray oscilloscope, while the other pair of plates were supplied by the maximum voltage being used in the experiment. A balance was achieved between the probe and standard signal when a horizontal line was obtained on the cathode-ray-oscilloscope screen.

The comparative simplicity of this part of the apparatus arises from the fact that a single probe was used. For the measurement of potential gradients, a more complicated circuit would be required.

Automatic field plotters have been designed in the past[17, 18]. In the calculator, potential measurements over the planform rather than around it were required, and so eliminated such devices.

4.6. *The Model.*

The part of the circuit representing the aerofoil and its wake may be described as the model. The assumptions and conditions necessary to realise the analogies have already been enumerated. The use of two analogies meant that the construction of the model depended upon the method of analysis.

Thus, when the direct analogy was to be used, provision had to be made for feeding a calculated current into given parts of the wing surface. The Kutta-Joukowsky condition required that the potential along the wake for any given value of the co-ordinate y should be constant and equal to that at the corresponding trailing-edge position. Finally the area outside the wing-wake region had to be at the same potential as the top electrode.

If the transverse analogy was employed, then the wing surface had to be an insulating area. The Kutta-Joukowsky condition involved the same preparation as in the direct analogy. Again, the condition outside the wing-wake area was that it should be at the upper-plate potential.

The form of models eventually employed in the two analogies are shown by Figures 3 and 7. The size of the tank restricted the model dimensions, which governed the cut to be made in the top electrode. Finally, a cut of 51 in. × 12 in. was decided upon.

All the models for this programme have been manufactured from sheets of Perspex. Its choice depended upon the following factors. It could be obtained in large sheets with a reasonable tolerance on its thickness, also it was easily machined and scribed. Scribing was employed to mark out areas that were to be conducting.

The conducting areas of the model were prepared by the following technique. The areas that were to be insulating zones were covered with strips of Sellotape. If any of the adhesive tape covered the conducting area, it was removed by using a razor blade and straight-edge. A silver-base conducting paint was then sprayed on to the model. The spraying was accomplished by the use of a small Aerograph spray gun and air compressor, with a working pressure of 40 lb/in.^{2}. Generally three coats of paint were adequate to produce a smooth finish. Finally, when the paint had dried, the Sellotape was removed, producing models similar to those in Figures 14 and 15. The dark areas represent insulating zones, the lighter regions are the conducting areas.

Greater accuracy is obtained with the calculator if:

(*a*) In the direct analogy, electric currents are fed in at a larger number of electrodes.

(*b*) The wake region is divided into a larger number of parallel lines (y = a constant), maintained at constant potential. This condition would apply for both the direct and transverse analogy.

Conditions (*a*) and (*b*) were approximated to as follows. The wing was divided up into discrete areas *ds* (Figure 3) and the electrical current satisfying the boundary condition at the centre of this area was applied *via* small brass electrodes. The electrodes were carefully machined flush to the base of the model to prevent any field distortion due to local variations in depth of the electrolyte (Figure 16).

The wake region was approximated to by a series of parallel strips (Figures 3 and 7). Each of the conducting areas and strips were separated by an insulating zone (Figure 17). The ratio of the conducting to insulating area has been laid down by previous workers.[6].

The opportunity was taken to investigate the significance of the approximations (*a*) and (*b*), which are similar to those met in the application of finite-difference methods. The results obtained from this programme have indicated general model electrode effects which will influence future model design.

The model was constructed in two parts. The rear part was purely representative of the wake. It could therefore be used in conjunction with models of different planforms. The front of the model constituted the planform, with a short section of the wake represented. The two halves were connected electrically *via* two rows of electrodes, placed in the wake (Figure 18).

Generally, potential measurements were taken at 121 stations. These stations resulted from dividing the wing into 11×11 chordwise-spanwise co-ordinates. The distribution of stations depended to some extent on the planform employed. For example, at the trailing-edge tips of delta wings, the concentration of stations was increased.

Two sides of the model were supported by the tank walls, and the remaining two by the upper electrode. The supports consisted of Perspex brackets into which were screwed brass levelling pins (Figures 14 and 15).

In the transverse analogy the stations consisted of $\frac{1}{8}$ in. diameter holes drilled in the Perspex. The dimensions of the conducting areas in the direct analogy depended on the planform being investigated. When using the transverse analogy, probes such as those shown in Figures 11 and 12 were placed in the station holes to obtain the potential distribution. Potential measurements were taken from the small electrodes, used for applying the boundary condition in the direct analogy.

The size of the wing area depended on the planform but all semi-spans of the models tested were less than or equal to ten inches.

4.7. *Apparatus for Establishing Boundary Conditions.*

In the analogies a means of varying the potential in the wake was necessary to establish the Kutta condition. This was achieved by placing 10,000 ohms, helical wound potentiometers, across the a.c. supply (Figure 4). This with the previously described apparatus was sufficient to set up the transverse analogy.

To complete the direct analogy, a further component was constructed. This consisted of an auxiliary-resistance network, which enabled the wing-current boundary condition to be applied (Figure 19).

4.8. *Procedure for Conducting an Experiment.*

The upper electrode was carefully levelled after which the tank was filled with water until it touched the bottom of the upper electrode. The water was then well stirred, and any air bubbles removed from under the top electrode. These bubbles were eliminated to prevent any field distortions.

The model was now placed in the tank and carefully levelled. Again care was taken to eliminate air bubbles. The depth of water was adjusted for the transverse analogy so that water was not drawn right up the station holes in the Perspex. A small syringe effectively controlled this factor.

The electrical circuit was then completed according to the analogy being used. The first operation was to satisfy the Kutta condition. When this was achieved the potential distribution over the wing surface was taken.

After the depth of water had been measured, the foregoing procedure completed an experiment using the transverse analogy. If, however, in the direct analogy, any potential on the wing was greater than 2% of the applied voltage V, then the potential difference across the resistance feeding the electrode was varied to obtain a better approximation to the tangential-flow condition.

The necessity for this adjustment arises because the presence of a finite voltage in the tank means that the tangential-flow condition is not accurately satisfied as shown by equation (40). In order to solve a problem by the direct analogy the condition expressed by equation (19) can only be approximated to when using the method of large resistances. By preventing the occurrence of potentials greater than 2% of the applied potential, a compromise is obtained between obtaining voltages which can be measured and approximating to the tangential-flow condition.

After the adjustment of the potentials feeding the large resistances, a check was made on the Kutta condition and a second potential distribution taken. After some experience it was possible to choose the resistances required to ensure a satisfactory result from the second potential-distribution measurement.

Before the results of the direct analogy could be converted into terms of the velocity potential, the conductivity of the water had to be measured. This was achieved by using the tank as a resistance in a Wheatstone bridge, and measuring the resistance. Knowing its dimensions and resistance, the conductivity of the volume of water was computed.

During an experiment both the air and water temperatures were taken to give an indication of the conditions of the test. This was necessary as a temperature effect was detected early on in the work which will be described later.

5. *Development of the Experimental Technique.*

The following sections deal with tests, designed to investigate a few of the factors, affecting the operation of a deep electrolytic tank. This was thought to be essential, as no previous experience of this particular method existed in the department.

The conditions aimed for were a quick simple method of simulating the lifting surface. The major portion of the preliminary investigations, were carried out in conjunction with the development of the transverse analogy.

5.1. *Bridge Faults.*

At the outset, it was found that the potential distribution was dependent upon the supply frequency.

The fundamental reasons for the dependence are unbalanced reactances. These may arise within the bridge circuit due to bad layout, earth capacitance effects or poor contacts.

The reduction of circuit inductances was a practical proposition and was accomplished by avoiding loops in the leads. All leads were shielded to avoid the effect of any variation in the external field.

Earth capacitance links give rise to a flow of current from the tank to earth, thus giving rise to an error in the measured voltage, even at balance. It was difficult to rationalise an approach to this problem, and a trial and error method was adopted. Thus the out-of-phase voltage was shown up on the cathode-ray oscilloscope, and the effect of touching various leads and pieces of apparatus noted. Then by shielding or inter-connecting, any change was observed. In this way the capacitance effects were reduced to a level where they were unimportant, or balanced out by the potentiometer capacitor circuit previously mentioned.

The presence of a poor contact was immediately registered on the cathode-ray oscilloscope as an ellipse. The contact could generally be quickly traced and rectified. To reduce the incidence of the aforementioned arising during a test, periodic checks were made on all connections.

5.2. *The Electrolyte.*

For reasons already given, the electrolyte decided upon was the Birmingham public water supply.

If the water was allowed to stand any appreciable time, a scum formed over the lower electrode. Analysis showed this to be silica, and as it is a good insulator would have tended to decrease the potentials within the tank. The water was changed every three weeks and during this period was well stirred before every test. Conductivity measurements taken over a period of four days when the water temperature varied by 0·2°C, showed an increase in conductivity of 2·4%. It was decided to investigate the effect, if any, of the conductivity of the electrolyte.

The experiment consisted of the analysis of an unswept rectangular wing of aspect ratio six using the transverse analogy. The analysis was performed with two separate electrolytes. Staffordshire tap water was imported, the relationship between the two waters being

$$\frac{\text{Resistivity of Birmingham water}}{\text{Resistivity of Staffordshire water}} = \frac{8}{1}$$

The results obtained were:

$\frac{dC_L}{d\alpha}$	Electrolyte
4·14	Birmingham water
4·21	Staffordshire water

The conductivity of the water, therefore, appears to influence the result.

It was essential to ensure no field distortions occurred, through air bubbles forming on the underside of the top electrode, or the upper surface of the lower electrode. By placing a cover over the tank during the night, the bubbles were drawn up to the underside of the top electrode. A wooden lath was then used to sweep the under surface, and in this manner all the air bubbles could be eliminated.

A further precaution that had to be taken concerning the electrolyte was the elimination of any local variation in conductivity. To this end the leads to the bottom electrode were sealed with an Araldite compound. The sealing compound used in the tank joints was selected so that it did not react chemically with the water. Because there might be a gradual dissolving of the electrode, the water was stirred vigorously. It was also essential to prepare the model in such a way that a minimum amount of silver paint flaked off when the model was placed in the tank.

The other property of the electrolyte affecting tank operation was its surface tension. No attempt was made to reduce the surface tension by wetting agents[20].

5.3. *The Electrodes.*

For the electrodes, three different materials were employed: brass, aluminium alloy and stainless steel. The upper plates were of the order of $\frac{1}{2}$ in. in thickness, the lower ones being about 0·06 in. thick.

Basically the electrode material should be a good conductor and corrosion resistant. The aluminium alloy became pitted in a short time, and on this account was discarded. The behaviour of the other two materials was more satisfactory but a greater capacitance component was noticed with the stainless steel. The brass electrode was used for most of the work.

Several workers[11, 12] give details of electrode preparations to reduce polarization. Amongst these is the use of a colloidal graphite. On account of the difficulty of obtaining a uniform layer and preventing the accidental removal of the graphite, it was decided to work with an untreated brass electrode system.

If the electrodes were allowed to stay in the tank too long, they became dirty and the problem of air bubbles adhering to their surface increased. The plates were therefore removed periodically to be cleaned.

The general conclusions drawn from this part of the investigation are in close agreement to those in Ref. 12. Namely the errors due to electrode-electrolyte combinations are probably small and cleanliness is of some importance.

Baker [21] thought that the probes were the most important source of error due to polarization and the probes were therefore coated in colloidal graphite.

5.4. *The Tank.*

If the tank were a poor insulator, field distortions would arise. To make an arbitrary assessment of the tank's insulating properties, the outside of the tank was further shielded by Perspex sheets. No difference in the potential field was noted and on this account the insulating property of the tank was deemed to be satisfactory.

5.5. *The Probe.*

The two-probe systems used in this work are shown in Figures 11 and 12. A comparison of the two probes during several tests showed no difference in performance and, due to its ease of construction, that shown in Figure 12b was mainly employed.

In the transverse analogy a potential is applied across the upper and lower electrodes of the tank and potential measurements taken in the plane $z = 0$. A potential gradient therefore exists in the z direction, and it was decided to investigate the order of this gradient, close to the under surface of the model.

It was realised that the height of water drawn into the model (Figure 21) might also affect the results and so tests were carried out in two parts.

First treated were the probe immersion factors. A delta wing of aspect ratio 1·848 was used in this investigation. It had previously been noted that the magnitude of the voltage variations occurring in these preliminary tests, varied along the spanwise direction. The probe investigation was therefore carried out at the stations $\eta = 0{\cdot}2$ and $\eta = 0{\cdot}6$ to obtain average values of the variations that might be expected to arise.

The model was placed in the tank and no attempt made to control the height of water within the station holes. The applied excitation was 25 volts, the frequency of excitation being 1,000 c/s. The Kutta condition was established and the trailing-edge potentials measured (Table 1).

A small rigid piece of wire was now fixed on to the probe which, with a depth gauge allowed the change in penetration to be measured (Figure 21). The results are tabulated in Table 1. As can be seen within the distorted region of the hole, the potential gradient is large. This region must therefore be avoided if consistent results are to be obtained.

The effect of controlling the height to which water was allowed to rise in the model, was carried out using an aspect-ratio 2 unswept rectangular wing. The Kutta condition was established and the T.E. potentials were measured. A known volume of water was removed and the T.E. potentials

again taken. The results are shown in Table 2. As the results show there was very little effect until 1,200 c.c. had been removed, when a significant drop in the level of water at the stations was observed. The results can be explained by the retention of the water within the holes, due to surface tension. The operating conditions were 25 volts at 1,000 c/s.

After the removal of 1,200 c.c. of water the Kutta conditions were re-established (Table 2). The following day the experiment was repeated. The results are shown in Table 2.

As a result of these tests the procedure for conducting an experiment became:

1. Levelling the top electrode.
2. Ensuring the model was horizontal.
3. Adjusting the depth of water to the required level.
4. Immersing the probe just below the under surface of the model.

5.6. *The Model.*

If the silver paint, representing the conducting areas, was sprayed on the model without any extra treatment, a large proportion was flushed off when first placed in water. This had to be avoided as it meant cleaning the water surface before the test could proceed.

It was found that by rubbing each coat of paint with a fine cloth, the next layer adhered to the Perspex more firmly. If when the final coat was dry the model was washed thoroughly, then flaking off was reduced.

5.6.1. *Smooth outflow.*—The model representation of the Joukowsky condition is an approximation in that:

1. The wake region was divided into a finite number of strips.
2. The trailing-edge potential was not measured at the true trailing-edge position.
3. The potential along a wake division could vary as a result of the surface impedance of the paint.

The approximation (1) has been investigated by Malavard[6]. As a result, the ratio of insulating to conducting area, shown in Figure 17 was recommended. Different divisions have been used during this work and the ratio of conducting length to insulating length has emerged as a significant factor. The potential distributions for an aspect-ratio 2 unswept rectangular wing with a 5% flap are shown in Table 3 for ratios of $\frac{\text{conducting length}}{\text{conducting length}+\text{insulating length}}$ of 0·7/1 and 0·925/1. The larger potential values refer to the ratio 0·7/1.

Models were prepared with trailing-edge stations as in Figure 22. Similar results were obtained for all the models and subsequently models were constructed with trailing-edge stations placed as in Figure 22b.

Several resistance readings gave an average value of 0·5 ohms for a strip of the conducting paint on Perspex, with dimensions as in Figure 23. No potential drop could be measured along the model wake strips.

5.6.2. *Model scale.*—The dimensions of the cut in the upper electrode provided a maximum gap between the plate and the model of 0·2 inches. Providing this gap did not exist in the region of high potential, namely the tank boundary, no distortion of the field occurred. The model was required therefore to butt tightly against the tank boundary.

An experiment was devised to estimate the result of varying model size. Two models of an unswept rectangular wing aspect ratio 2 were prepared. One with a semi-span of 9·6 in. the other one of

4·8 in. The results are shown in Table 4. The overall effect is a decrease in $dC_L/d\alpha$ of 3·8%, with decrease in span. Model size does not account for all of this change because of the more coarse wake division in the smaller model.

A further factor investigated was the length of wake region used. Thus with an aspect-ratio 2 unswept rectangular wing, two sets of readings were taken for the trailing-edge potentials with wake lengths shown in Table 4.

The shortening of the wake region is equivalent to reducing the length of wind-tunnel section behind a model where vorticity is permitted. The figures of Table 4 show the circulation to be greater for the smaller wake. An approximate fourfold increase in wake length produced a decrease in circulation of the order of five per cent.

5.6.3. *Behaviour of model as an electrode.*—During the initial work on the direct analogy it was noticed that the magnitude of the out-of-phase voltages varied from one conducting area to another. As a result of a closer investigation this factor was broken down into two parts.

Firstly, the way in which the brass electrode was inserted into the model proved important. If not inserted flush with the under surface of the model, then a noticeable out-of-phase voltage was recorded (Figure 24).

Secondly, a circuit shown in Figure 25 proved that the silver-painted areas provided a surface-impedance effect. The proof being shown by the requirement of a resistance-capacitance bridge arm to balance the electrode signal.

The first factor was overcome by machining the electrodes flush to the under surface. The second was similar to the main electrode surface-impedance effect.

5.7. *Temperature Effects.*

5.7.1. ΔT *tests.*—It was thought possible that temperature variations between the water and surrounding air might exist. Therefore, a controlled experiment was devised to investigate the results of such temperature gradients.

A rectangular wing of aspect ratio 6 was used for the first part of the test. The air temperature was measured at a point 8 in. above the middle of the upper plate. The water temperature varied little and the point of measurement was arbitrary.

To enable a quick measurement of the potentials, readings were taken at the stations $\eta = 0{\cdot}02$ and $\eta = 0{\cdot}1$. The average of the values obtained for different values of ΔT, are shown in Table 5. ΔT was the parameter chosen to represent the temperature effect where ΔT = (water temperature, T_w) − (air temperature, T_a).

Three tests were then carried out with different values of T_w but with $\Delta T = 0$. The results are shown in Table 5 and Figure 34 and demonstrate the independence of the potential distribution on the water temperature.

A detailed explanation of the ΔT test is not possible. The mechanism that takes place may be as follows. The thermal conductivity of slate is small compared with brass, $4{\cdot}7 \times 10^{-3}$ to $2{\cdot}6 \times 10^{-1}$. Any heat exchange due to a difference in T_w and T_a will then be mainly through the upper electrode. The electric conductivity of tap water varies inversely as the temperature. Thus, depending on whether ΔT is positive or negative, there will be a local change in conductivity near to the upper electrode. As a result the field near the model will be disturbed and this could explain the variations due to the temperature gradients.

A further test was carried out using the delta wing model of aspect ratio 1·848. ΔT was varied, but the duration of these tests were shorter than those described above and a steady state was not attained. The results are shown in Table 6. They still show a small temperature dependency.

As a result of these tests, it appeared that providing temperature conditions remained constant during an experiment, no corrections need be made to the results. Fortunately, under working conditions ΔT was very nearly zero.

5.7.2. *Drift.* A secondary feature of electrolytic tanks investigated was drift. This is the change in potential from the just-switched-on position to the stabilised value.

The results were obtained from an experiment run on the rectangular wing aspect ratio 6 and are shown in Table 7. As can be seen drift is of second-order importance. Providing the current was switched on for two or three minutes before proceeding with the experiment no further precaution was required.

5.8. *D.C. Circuit Test.*

The behaviour of the tank using d.c. excitation was investigated. A simplified diagram of the circuit is shown in Figure 26. The applied excitation was 14·5 volts and the current taken was 60mA.

It was impossible to find a steady balance point, but Lingane[22] recommends excitation in the region of 140 volts, if d.c. is used. The difficulty of finding a balance point was indicated by the continual movement of the galvanometer spot. The spot moved across the scale in twenty minutes, which was too short a time for establishing boundary conditions and taking readings of the potential.

The higher voltages as recommended above were not tried, and the experiment was abandoned.

5.9. *Conductivity Measurements.*

Originally it was intended to use a small cell as designed by Malavard[6] for conductivity measurements, Figure 27. Towards this end the cell was calibrated at 19°C, and the results are shown in Figure 35.

Because of the low conductivity of the Birmingham tap water standard solutions with similar values could not be easily prepared. Furthermore it was realised that calibration of the cell must be carried out at different temperatures. The cell only measured local conductivity. It was also possible that if submerged to any great depth in the tank, the calibration constant might vary, due to the greater hydrostatic pressure forcing in more of the electrolyte.

On account of these reasons conductivity of the water was finally determined by using the tank as the unknown arm in a Wheatstone Bridge, Figure 28. This method proved satisfactory, and detected day to day variations of conductivity. Furthermore, no temperature calibration was required, and the average conductivity of the tank's contents were measured.

When using the tank for conductivity measurements the cut in the top electrode was filled in by a conducting sheet of Perspex. A capacitor was also required to obtain a sharp balance position.

5.10. *Development of the Technique of Large Resistances.*

In the direct analogy it was necessary to establish the condition as expressed by equation (*a*) on the wing, Figure 29.

$$m \frac{dV}{dz} = - U\beta. \qquad (a)$$

The current passing into an area dx, dy is

$$i = -\frac{dV}{dz} dx\, dy\, \sigma . \tag{b}$$

If a large resistance is used then

$$i = \frac{V - v}{R_L} \simeq \frac{V}{R_L} . \tag{c}$$

The relationship between the velocity potential ϕ and the electrical potential V in this case is

$$\phi = mV , \tag{d}$$

then

$$m = \frac{R_L U \beta\, dx\, dy\, \sigma}{V} . \tag{e}$$

5.10.1. *Initial tests.*—It was realised early on, that the conductivity of the Birmingham tap water was of such an order that the technique of large resistances would be difficult to apply. This difficulty occurs because for any given problem, as the conductivity of the electrolyte decreases, so the potentials within it must increase. This follows as m is directly proportional to σ.

The technique is satisfactory providing the potentials within the tank are small, and this condition requires that m should be correspondingly large.

The obvious ways of doing this were to increase one of the following, R, $dx\, dy$ or σ.

The conductivity of the electrolyte was fixed. The area $dx\, dy$ was also fixed within narrow limits if a good approximation to the wing surface was to be achieved. The only method available therefore was to experiment with different values for R_L.

A rectangular wing of aspect ratio 2, with a flap 5% of the chord was chosen. The wing boundary condition was established by means of $\frac{1}{2}M\Omega$ and $1M\Omega$ resistances respectively. The results for the trailing-edge potentials are shown in Table 8. The results showed that if the tank potentials were to be suppressed to within 2% of the applied potential then resistances of the order of $1M\Omega$ had to be employed.

Much of the work carried out involved plane flap control surfaces. This meant that the same current had to be fed into each electrode station. Three possibilities then arose at this stage to achieve this condition:

1. Use large enough equal resistances for model potential to be insignificant.
2. Use smaller equal resistances and vary the applied potential.
3. Use resistances of different values to simulate condition (2).

Of these the first and third were the easiest to apply in practice. These two methods were used on all the plane surface control problems. Thus it was known that the potentials decreased in general, from the root chord position to the wing tip. Also the potentials decreased from trailing edge to leading edge.

$1M\Omega$ resistances were graded, by means of a Wheatstone Bridge Post Office circuit, into values which varied by 1%. The smaller resistances would then feed the regions of high potential in the tank.

A series of tests was now planned to determine the behaviour of the methods in practice. An unswept rectangular wing of aspect ratio 2 was used in the series. At first the bottom plate was not connected in the circuit, and the T.E. potentials for a full span 5% flap, as shown in Table 9 resulted.

The upper and lower plates were then connected, and the potentials of Table 9 were read. This connection is therefore of some significance, and must be made for the application of the correct boundary conditions.

T.E. potential measurements were now read at different frequencies and magnitudes of excitation (Table 9). As can be seen from the table, the results were independent of frequency. Any change in conductivity resulted in a change of potentials, such that the aerodynamic parameters calculated were independent of this change.

5.10.2. *Plane surface control tests.*—A few of the practical observations made during this part of the work will now be enumerated.

I. Because of the low voltages being measured, the potentiometer capacitor circuit was not required in the null-indicator circuit.

II. Only those resistances being used during an experiment should have a voltage applied to them. This was necessary as any excess resistances gave rise to an error signal.

III. All electrodes should be of the same shape and dimensions if possible. Thus, when the delta wing of aspect ratio 2 was designed, arrangements were made for representing full-span local-chord and root-chord flaps as well as an all-moving tip. As a consequence different sizes and shapes of electrodes resulted. Resistances corresponding to the different areas were chosen, but on measuring the potential distribution it was found to be irregular. Therefore any form of plane control surface should be represented by regular sized parallelograms if the technique is to be successful.

5.10.3. *The cambered wing.*—The ultimate development of the method of large resistances was to represent thin wing forms of any given camber. The wing chosen to investigate the method was a 45% swept constant-chord wing of aspect ratio 4. The camber distribution as shown in Figure 30 applied for each chord section.

Because the surface camber varied then varying resistances had to be employed. As a first choice the largest resistance used was $2M\Omega$. An initial potential distribution was taken to see how far the boundary condition was satisfied. The potentials across the large resistances were then varied to give a better approximation.

The circuit diagram used for this section of the work and a general view of the apparatus are shown in Figures 31 and 19. This method of choice of resistances, and then variation of potential, proved to be quite satisfactory in practice.

6. *The Programme of Work.*

The following programme was laid down within which the development of the lifting-surface calculator was to be attempted.

6.1. *Plane Lifting Surfaces.*

I. Unswept rectangular wings; aspect ratios of 6, 4, 2 and 1.

II. Constant-chord wing; 45° sweep; aspect ratio 4.

III. Delta wings; aspect ratios of 2 and 1·848.

6.2. *Plane Lifting Surfaces with Flaps.*

I. Unswept rectangular wings.

(*a*) 15% chord full-span flap.

(*b*) 25% chord full-span flap. Aspect ratios of 4, 2 and 1.

(*c*) 35% chord full-span flap.

II. Constant-chord wing; 45° sweep; aspect ratio 4.

(*a*) 25% chord full-span flap.

III. Delta wing; aspect ratio 2.

(*a*) full-span flap, 5% of root chord.

(*b*) full-span flap, 10% of root chord.

(*c*) full-span flap, 15% of root chord.

(*d*) full-span flap, 15% of local chord.

(*e*) all-moving tip outboard of 0·67 semi-span.

(*f*) all-moving tip outboard of 0·74 semi-span.

6.3. *Thin Cambered Wing.*

1. L'Aile I. Ref. 23.

7. *Discussion.*

A comparison between the results obtained for the unswept plane rectangular wings and the constant-chord plane wing, shows good agreement with those published in References 23, 24 and 25.

The values of the lift coefficients of the plane delta wings of aspect ratios 1·848 and 2 are smaller than those published in Reference 26. As already indicated the results obtained for the delta wing with control surfaces cannot be viewed with any confidence. In the case of the full-span flaps, the varied shapes and sizes of the conducting areas complicated the tangential-flow condition and resulted in an irregular potential distribution. The results obtained for the all-moving tip outboard of 0·67 of the semi-span are more reliable, as the conducting areas are more uniform in size and shape. The test for the tip outboard of 0·74 of the semi-span was not satisfactory because of its poor definition, i.e., too few conducting areas. Results from tank tests carried out by Malavard *et al.*[26] have been used by Brebner and Lemaire[29] to calculate the spanwise loading of swept-back wings with all-moving tips.

The model used in the analysis of the cambered constant-chord wing had its leading-edge stations at $\eta = 0{\cdot}05$ and the trailing-edge position $\eta = 0{\cdot}95$. Furthermore, the wing surface was only divided into one hundred stations. These facts would account for the experimental values being lower than those published in References 23 and 27. Experience from the work indicates that a finer network of stations would increase the experimental values obtained here.

As a result of this initial work the transverse analogy is well established and can now be used for the analysis of more-complicated wing forms. Use of the direct analogy can also now be extended to more-complicated problems provided careful consideration is given to model design.

8. *Tables of Results.*

UNSWEPT RECTANGULAR WINGS.

(*a*) *Plane Lifting Surfaces.*

Aspect Ratio	$\partial C_L/\partial\alpha$		
	Experiment	Falkner	Richards
1	1·47	1·49	1·46
2	2·45	2·52	2·47
4	3·62	3·64	3·56
6	4·13		

The theoretical values quoted above are due to Falkner (Ref. 24) and Richards (Ref. 25).

(*b*) *Plane Wing at Zero Incidence with Deflected Flaps* (Full span).

Aspect Ratio 1	$\frac{\partial C_L}{\partial\alpha}$	Aspect Ratio 2	$\frac{\partial C_L}{\partial\alpha}$	Aspect Ratio 4	$\frac{\partial C_L}{\partial\alpha}$
c'/c		c'/c		c'/c	
15%	0·700	15%	1·20	15%	1·62
25%	0·920	25%	1·54	25%	2·11
35%		35%	1·77	35%	2·46

CONSTANT CHORD 45° SWEEP BACK.

(*a*) *Plane Lifting Surfaces.*

Aspect ratio	$\partial C_L/\partial\alpha$		
	Experiment	Duquenne	Falkner
4	2·95	3·05	2·99

The value obtained is compared with an experimental value due to Duquenne[23] and a theoretical value by Falkner[2].

UNSWEPT RECTANGULAR WINGS.

(*a*) *Plane Lifting Surface.*

Aspect Ratio 1

η	0·05	0·15	0·25	0·35	0·45	0·55	0·65	0·75	0·85	0·95
C_l/C_L	1·27	1·26	1·24	1·20	1·14	1·07	1·0	0·85	0·68	0·40

Aspect Ratio 2

η	0·02	0·1	0·2	0·3	0·4	0·5	0·6	0·7	0·8	0·9	0·98
C_l/C_L	1·26	1·25	1·23	1·21	1·17	1·10	1·03	0·927	0·790	0·583	0·327

Aspect Ratio 4

η	0·02	0·1	0·2	0·3	0·4	0·5	0·6	0·7	0·8	0·9	0·98
C_l/C_L	1·26	1·25	1·24	1·22	1·18	1·14	1·08	0·985	0·857	0·651	0·389

Aspect Ratio 6

η	0·05	0·15	0·25	0·35	0·45	0·55	0·65	0·75	0·85	0·95
C_l/C_L	1·18	1·18	1·16	1·14	1·11	1·07	1·01	0·92	0·77	0·49

(*b*) *Surface with Deflected Flaps* (Full Span).

Aspect Ratio 1

	η	0·05	0·15	0·25	0·35	0·45	0·55	0·65	0·75	0·85	0·95
$\frac{C_l}{C_L}$	$c'/c = 15\%$	1·246	1·239	1·224	1·187	1·143	1·085	0·997	0·872	0·704	0·425
	$c'/c = 25\%$	1·248	1·242	1·225	1·191	1·141	1·075	0·975	0·847	0·674	0·401

Aspect Ratio 2

	η	0·02	0·1	0·2	0·3	0·4	0·5	0·6	0·7	0·8	0·9	0·98
$\frac{C_l}{C_L}$	$c'/c = 15\%$	1·191	1·225	1·196	1·174	1·144	1·093	1·033	0·956	0·837	0·649	0·389
	$c'/c = 25\%$	1·199	1·202	1·199	1·179	1·146	1·092	1·029	0·945	0·822	0·628	0·367
	$c'/c = 35\%$	1·223	1·228	1·223	1·199	1·159	1·101	1·028	0·935	0·802	0·604	0·351

Aspect Ratio 4

	η	0·05	0·15	0·25	0·35	0·45	0·55	0·65	0·75	0·85	0·95
$\frac{C_l}{C_L}$	$c'/c = 15\%$	1·166	1·184	1·176	1·156	1·126	1·084	1·016	0·924	0·774	0·466
	$c'/c = 25\%$	1·164	1·180	1·170	1·154	1·124	1·078	1·010	0·910	0·752	0·442
	$c'/c = 35\%$	1·190	1·204	1·192	1·174	1·148	1·100	1·026	0·918	0·748	0·430

CONSTANT CHORD 45° *SWEEP.*

(*a*) *Plane Lifting Surface* (Aile '0').

Aspect Ratio 4

η	0·05	0·15	0·25	0·35	0·45	0·55	0·65	0·75	0·85	0·95
C_l/C_L	1·05	1·09	1·12	1·14	1·14	1·12	1·08	1·00	0·840	0·480

(*b*) *Surface with Deflected Flap* (Full Span).

Aspect Ratio 4

	η	0·05	0·15	0·25	0·35	0·45	0·55	0·65	0·75	0·85	0·95
$\frac{C_l}{C_L}$	$c'/c = 20\%$	0·966	1·20	1·26	1·30	1·32	1·32	1·30	1·22	1·06	0·697
	$c'/c = 30\%$	0·956	1·03	1·08	1·11	1·13	1·12	1·10	1·03	0·886	0·565

(*c*) *Surface with Deflected Flap* (Outboard 0·5 semi-span).

Aspect Ratio 4

	η	0·05	0·15	0·25	0·35	0·45	0·55	0·65	0·75	0·85	0·95
C_l/C_L	c'/c 30%	0·166	0·196	0·256	0·392	0·702	1·51	1·85	1·96	1·80	1·22

(*d*) *Cambered Wing* (Aile 1).

Aspect Ratio 4

η	0·05	0·15	0·25	0·35	0·45	0·55	0·65	0·75	0·85	0·95
C_L	0·229	0·248	0·261	0·270	0·275	0·278	0·275	0·262	0·233	0·158
C_{LO}	0·235	0·260	0·275	0·282	0·287	0·289	0·287	0·270	0·242	0·172
C_{LK}	0·187	0·232	0·263	0·277	0·283	0·285	0·285	0·283	0·275	0·210

C_{LO} refer to the results obtained by Duquenne[23].

C_{LK} refer to the results obtained by Küchemann[27].

DELTA WINGS.

(*a*) *Plane Lifting Surface.*

Aspect Ratio 1·848

η	0·025	0·1	0·2	0·3	0·4	0·5	0·6	0·7	0·8	0·9	0·975
C_l/C_L	1·25	1·245	1·24	1·22	1·20	1·16	1·04	0·880	0·760	0·496	0·236

(*b*) *Surface with Deflected Flaps* (Full span).

Aspect Ratio 2

	η	0·05	0·15	0·25	0·35	0·45	0·55	0·63	0·70	0·77	0·85	0·95
$\frac{C_l}{C_L}$	5% root chord	1·48	1·75	1·18	1·12	1·32	0·959	0·978	0·649	0·689	0·613	0·383
	10% root chord	1·30	1·35	1·12	1·08	1·22	0·981	1·01	0·994	0·775	0·634	0·366
	15% root chord	1·28	1·32	1·12	1·09	1·22	1·00	1·02	1·00	0·787	0·630	0·362
	15% local chord	1·50	1·53	1·25	1·16	1·33	0·933	0·879	0·582	0·553	0·475	0·283

(*c*) *Surface with All-Moving Tip.*

Aspect Ratio 2

	η	0·05	0·15	0·25	0·35	0·45	0·55	0·63	0·70	0·77
$\frac{C_l}{C_L}$	Outboard 0·67 semi-span	0·560	0·560	0·608	0·667	0·763	0·954	1·23	2·04	1·68
	Outboard 0·74 semi-span	0·530	0·530	0·553	0·576	0·645	0·760	0·922	1·15	2·17

Aspect ratio 2—continued

		η	0·85	0·95
$\frac{C_l}{C_L}$	Outboard 0·67 semi-span		1·59	0·854
	Outboard 0·74 semi-span		2·28	1·43

UNSWEPT RECTANGULAR WING.

(*a*) *Plane Lifting Surface.*

Pressure Coefficient C_p/α

Aspect Ratio 1

ξ \ η	0·3	0·5	0·6	0·7	0·8
0·2	1·03	0·956	0·805	0·719	0·694
0·3	0·656	0·592	0·586	0·533	0·380
0·4	0·268	0·390	0·427	0·317	0·273
0·5	0·280	0·280	0·275	0·259	0·185
0·8	0·185	0·173	0·146	0·164	0·167

Local Aerodynamic Centre χ_η/c

Aspect Ratio 6

η	0·2	0·4	0·6	0·8	1·0
χ_η/c	0·24	0·24	0·23	0·22	0·20

Aerodynamic Centre Behind L.E. 0·238*c*

Aspect Ratio 1

η	0·2	0·4	0·6	0·8	1·0
χ_η/c	0·187	0·189	0·189	0·189	0·180

(*b*) *Plane Surface with Deflected Flaps* (Full span).

Aspect Ratio 4·35% *Flap*

η \ ξ	0·4	0·5	0·6	0·7	0·8	0·9	
0·5	1·82	2·09	2·59	1·88	0·816	0·195	$\frac{C_p}{\alpha}$
0·95	0·466	0·485	1·17	0·858	0·338	0·141	

η	0·5	0·65	0·75	0·95
$\frac{\chi_\eta}{c}$	0·435	0·453	0·458	0·591

CONSTANT CHORD 45° *SWEEP.*

(*a*) *Plane Lifting Surface.*

Aspect Ratio 4

η \ ξ	0·1	0·3	0·5	0·7	0·9	
0·02	3·74	1·48	1·14	0·876	0·480	
0·30	2·46	1·41	0·942	0·708	0·253	$\frac{C_p}{\alpha}$
0·8	2·46	1·41	0·554	0·240	0	
0·98		0·240	0·116	0	−0·177	

Aspect Ratio 4

η	0·1	0·2	0·4	0·6	0·8	0·9
$\frac{\chi_\eta}{c}$	0·29	0·26	0·24	0·23	0·18	0·15

(*b*) *Cambered Wing*—(Aile 1) (Ref. 23).

Aspect ratio	$\partial C_L/\partial\alpha$		
	Experiment	Duquenne	Küchemann
4	0·252	0·262	0·262

The experimental value is compared with those due to Duquenne[23] and Küchemann[27].

DELTA WING.

(*a*) *Plane Lifting Surface.*

Aspect ratio	$\partial C_L/\partial\alpha$	
	Experiment	Malavard
2	2·13	2·24
1·848	2·10	2·13

The values are compared with that obtained by Malavard[26].

(*b*) *Plane Surface at Zero Incidence with Deflected Flaps* (Full span).

Aspect Ratio 2

	% Root chord	$\partial C_L/\partial\alpha$
I. *Root Chord Flap*	5%	1·09
	10%	1·57
	15%	1·81
	% Local chord	
II. *Local Chord Flap*	15%	1·38

		$\partial C_L/\partial\alpha$
III. *All-Moving Tip*	Outboard 0·67 of semi-span	0·408
	Outboard 0·74 of semi-span	0·211

9. *Conclusions.*

The application of the electrolytic tank to the solution of the plane lifting-surface problem has proved to be an accurate means of analysis. The technique is easily extended to compute the velocity-potential distribution over any geometrically shaped plane surface.

When using the direct analogy certain practical difficulties have to be overcome if satisfactory results are to be obtained. The difficulties occur for two reasons. Firstly, the potentials within the tank are small and secondly model design is of greater significance than in the transverse analogy.

Further refinements such as cathode followers would now provide a further improvement to the apparatus. Nevertheless in its present form the method could well be extended to the solution of more complicated problems than those treated here.

LIST OF SYMBOLS

AR		Aspect ratio
C_p		Pressure coefficient
b		Semi-span
c		Local chord
C_L		Overall lift coefficient
p		Local pressure
U		Free-stream velocity
u		Local velocity
LE		Leading edge
TE		Trailing edge
X, Y, Z		Cartesian co-ordinates
h		Depth of electrolyte
i		Electric current
R		Electric resistance
V		Electric potential
α		Surface incidence to free-stream velocity
β		Control surface angle of deflection
ρ		Density
η	$=$	y/b
ξ	$=$	x/c
Φ		Velocity potential
ϕ		Perturbation potential
χ		Aerodynamic centre
$Q(t)$		Mass of fluid at time t
S		Closed surface
a_∞		Free-stream sonic velocity
Γ		Circulation/unit span width
$l(\eta)$		Section lift
L		Overall lift
$m(\eta)$		Section pitching moment about y axis
M		Total pitching moment
σ		Conductivity of electrolyte
m		Dimensional constant

LIST OF SYMBOLS—*continued*

$F(xy)$	Equation of lifting surface
T_W	Water temperature
T_A	Air temperature
v	Volume
$\bar{A}$	Vector quantity
∇	Vector operator

REFERENCES

No.	*Author*	*Title, etc.*
1	L. C. Malavard	La methode d'analogie rheoelectrique, ses possibilités et ses tendances. *L'onde electrique.* Vol. 35. 1956.
2	V. M. Falkner	The calculation of aerodynamic loading on surfaces of any shape. A.R.C. R. & M. 1910. August, 1943.
3	D. Cohen	A method for determining the camber and twist of a surface to support a given distribution of lift, with applications to the load over a swept-back wing. N.A.C.A. Report 826. 1945.
4	R. S. Swanson and S. M. Crandall	An electromagnetic-analogy method of solving lifting-surface theory problems. N.A.C.A. ARR L5D23. (WR. L–120). May, 1945.
5	W. P. Jones	Theoretical determination of the pressure distribution on a finite wing in steady motion. A.R.C. R. & M. 2145. May, 1943.
6	L. C. Malavard	The use of Rheoelectrical Analogies in Aerodynamics. AGARDograph 18. August, 1956.
7	W. F. Campbell	Two electrical analogies for the pressure distribution on a lifting surface. N.R.C.C. Report M.A.—219. 1949.
8	W. B. Brower, Jr.	The application of the electric tank analogy to two and three dimensional problems in linearised aerodynamic theory. Rensselaer Polytechnic Institute. 1955.
9	L. C. Malavard and R. Duquenne	The investigation of lifting surfaces by a Rheoelectric Analogy. M.o.A. T.I.L. Trans. T. 3989. May, 1952.
10	W. J. Karplus	*Analogue simulation.* McGraw-Hill. 1958.
11	P. A. Einstein	Factors limiting the accuracy of electrolytic plotting tanks. *Brit. J. App. Phys.* Vol. 2. p. 49. 1951.
12	K. F. Sander and J. G. Yates ..	The accurate mapping of electric fields in an electrolytic tank. *Proc. Inst. Elec. Eng.* Vol. 100. Part II. 1953.

No.	*Author*	*Title, etc.*
13	J. C. Burfoot	Probe impedence in the electrolytic tank. *Brit. J. App. Phys.* Vol. 6. p. 175. 1955.
14	P. A. Einstein	Improved balance indication for bridge with Wagner earthing arms using a C.R.O. *J. Sci. Instrum.* Vol. 27. p. 27. 1950.
15	G. H. Rayner and R. W. Willmer	A method of decreasing the effect of earth admittances in A.C. bridges. *J. Sci. Instrum.* Vol. 27. p. 103. 1950.
16	A. R. Boothroyd, E. C. Cherry and R. Makar	An electrolytic tank for the measurement of steady state response, transient response and allied properties of networks. *Proc. Inst. Elec. Eng.* Vol. 96. Part I. p. 163. 1949.
17	P. E. Green	Automatic plotting of electrostatic fields. *Review of Scientific Instruments.* Vol. 19. p. 696. 1948.
18	R. B. Burtt and J. Willis	A high speed electronic analogue field mapper. *J. Sci. Instrum.* Vol. 34. p. 177. 1957.
19	B. Hague	*A.C. Bridge methods.* Pitman
20	D. McDonald	The electrolytic analogue in the design of high voltage power transformers. *Proc. Inst. Elec. Eng.* Vol. 100. Part II. 1953.
21	B. O. Baker	Automatic electron trajectory plotting using the electrolytic tank analogue. *Brit. J. App. Phys.* Vol. 5. 1954.
22	J. J. Lingane	*Electroanalytical chemistry.* Interscience Publishers, Inc. M.7.
23	R. Duquenne	Application de l'analogie rheoelectrique au calcul de trois ailes de meme forme en plan. O.N.E.R.A. N.T. M.9/1292A Aeronautiques. September, 1953.
24	V. M. Falkner	Calculated loadings due to incidence of a number of straight and swept-back wings. A.R.C. R. & M. 2596. June, 1948.
25	D. J. W. Richards	Aero/FM/Technical Report/003. 1959.
26	L. C. Malavard, R. Duquenne, M. Enselme and C. Grandjean	Proprietes calculées d'ailes en delta. O.N.E.R.A. N.T. No. 25. 1955.
27	D. Küchemann	A simple method for calculating the span and chordwise loadings on thin swept wings. A.R.C. 13,758. August, 1950.
28	O.N.E.R.A.	Calcul d'effects de volets par analogie rheoelectrique. O.N.E.R.A. No. 11/1292A. July, 1954.
29	G. G. Brebner and D. A. Lemaire	The calculation of the spanwise loading of sweptback wings with flaps or all-moving tips at subsonic speeds. A.R.C. 18,273. September, 1955.

TABLE 1

Probe Immersion Tests, A.R. 1·848

η	0·02	0·1	0·2	0·3	0·4	0·5	0·6	0·7	0·8	0·9	0·98	
T.E. Potential	2231	2215	2169	2100	1998	1865	1693	1477	1194	0811	0382	Before test
T.E. Potential	2231	2214	2170	2098	1995	1859	1684	1468	1187	0803	0380	After test

$\eta = 0·2$ T.E. Potential	Gauge reading (in.)	$\eta = 0·6$ T.E. Potential	Gauge reading (in.)
2140	0·1525	1675	0·1075
2148	0·1905	1678	0·1410
2156	0·2260	1682	0·1640
2158	0·2415	1683	0·1890
2160	0·2560	1684	0·1930
2162	0·3010	1685	0·2230
2164	0·3280	1686	0·2360
2165	0·3870	1688	0·2825
2168	0·4340		
2170	0·4785		

TABLE 2

Effect of Electrolyte Removal

c.c. removed	η	0·02	0·1	0·2	0·3	0·4	0·5	0·6	0·7	0·8	0·9	0·98	
0		2292	2279	2246	2194	2121	2020	1870	1681	1426	1051	0594	
100		2292	2281	2248	2195	2119	2017	1866	1678	1423	1051	0595	
400		2293	2281	2248	2195	2120	2019	1867	1679	1426	1052	0597	
900		2294	2284	2253	2199	2124	2023	1873	1686	1433	1062	—	
1200		2311	2300	2270	2218	2146	2046	1899	1713	1455	1083	0609	
1200		2308	2296	2267	2217	2150	2039	1883	1693	1435	1060	0606	K.J. re-established
		2311	2298	2269	2219	2152	2043	1887	1696	1435	1053	0605	following day.

TABLE 3

η	0·02	0·1	0·2	0·3	0·4	0·5	0·6	0·7	0·8	0·9	0·98
T.E. Potential	146	147	146	145	142	137	130	121	107	96	54
η	0·05	0·15	0·25	0·35	0·45	0·55	0·65	0·75	0·85	0·95	
T.E. Potential	131	132	132	129	125	119	112	101	85	57	

TABLE 4

Model Factors

η	0·02	0·1	0·2	0·3	0·4	0·5	0·6	0·7	0·8	0·9	0·98
Semi-span 9·6 in. wake 24½ in.	2311	2298	2269	2219	2152	2043	1887	1696	1435	1053	0605
Semi-span 9·6 in. wake 6 in.	2424	2412	2385	2336	2291	2177	1993	1790	1533	1125	0640
Semi-span 9·6 in. wake 24½ in.	1282		1256		1181		1044		0797		0221

TABLE 5

Aspect Ratio 6

ΔT	V	*Temp.* °C	15·8	17·3	19·0
10·0	1260·25	η	$\Delta T = 0$	$\Delta T = 0$	$\Delta T = 0$
7·0	1253·0	0·98	0442	0445	0447
3·1	1237·0	0·9	0726	0728	0731
1·2	1235·25	0·8	0930	0932	0935
0·15	1232·25	0·7	1052	1053	1056
−0·2	1233·5	0·6	1132	1133	1136
−0·3	1231·75	0·5	1183	1187	1190
−0·4	1231·75	0·4	1224	1225	1227
−0·65	1232·0	0·3	1251	1251	1252
−0·8	1233·25	0·2	1267	1268	1268
−1·2	1229·25	0·1	1277	1278	1278
−1·7	1227·75	0·02	1280	1282	1281
−2·15	1227·0				
−2·9	1227·0				
−2·5	1225·0				

TABLE 6

Aspect Ratio 1·848

Time	ΔT	$\eta = 0{\cdot}02$	$\eta = 0{\cdot}4$	$\eta = 0{\cdot}98$
0	−0·3	2248	2014	0394
25 min	−0·9	2248	2014	0394
40 min	−1·8	2248	2014	0394
52 min	−2·1	2248	2014	0393
1 h 45 min	−2·8	2247	2012	0393
2 h 45 min	−3·6	2245	2011	0393
3 h 30 min	−3·8	2244	2010	0393
4 h 5 min	−4·3	2244	2009	0393
5 h 35 min	−5·2	2243	2008	0393

TABLE 7

Temperature Tests

T	Drift
5·1	−0·5
3·0	+3·0
1·2	−0·5
0·6	−1·0
0·15	+1·0
0	−1·0
−0·2	0
−0·2	0
−0·3	−0·5
−0·3	−1·0
−0·5	−1·0
−0·8	−2·0
−1·2	−1·0
−1·2	−2·5
−2·1	−6·0
−5·0	−11·5
−5·0	−12·0
−6·0	−11·0

TABLE 8

η	0·02	0·1	0·2	0·3	0·4	0·5	0·6	0·7	0·8	0·9	0·98
$\frac{1}{2}M$	0594	0600	0594	0580	0554	0504	0454	0423	0337	0327	0215
$1M$	0325	0329	0327	0324	0316	0305	0290	0269	—	0182	0073

TABLE 9

Conditions of test / η	0·02	0·1	0·2	0·3	0·4	0·5	0·6	0·7	0·8	0·9	0·98
AR = 2. 5% Flap. 16·25V. 1000 c/s Electrodes unconnected	157	157·5	157	154	149	142	134	126	112	91	58
AR = 2. 5% Flap. 16·25V. 1000 c/s Electrodes connected	154	154	154	152	147	140	132	123	110	90	57
AR = 2. 5% Flap. 8V. 1000 c/s Electrodes connected	154	154	154	152	147	140	132	123	110	90	57
AR = 2. 5% Flap. 11·6V. 1000 c/s Electrodes connected	154	154	154	152	147	140	132	123	110	90	57
AR = 2. 5% Flap. 13·8V. 2000 c/s Electrodes connected	154	154	154	152	147	140	133	123	110	90	57·5

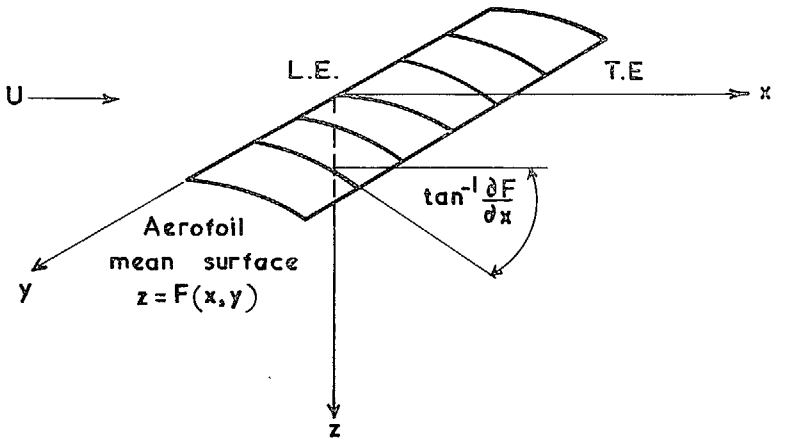

FIG. 1. Co-ordinate system.

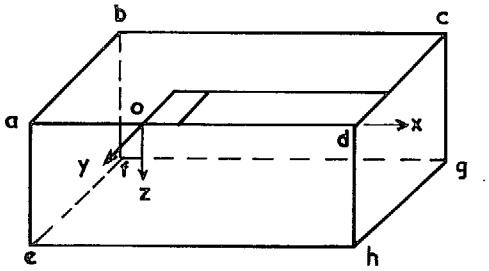

FIG. 2. The electrolytic field.

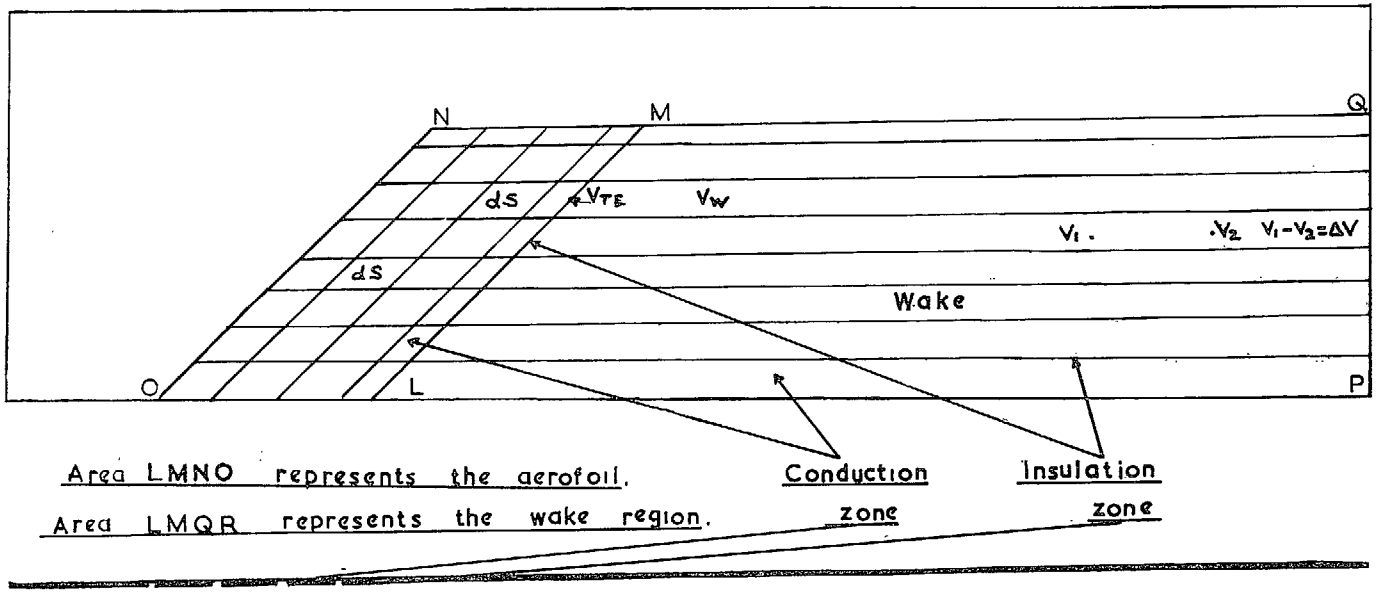

FIG. 3. The direct-analogy model.

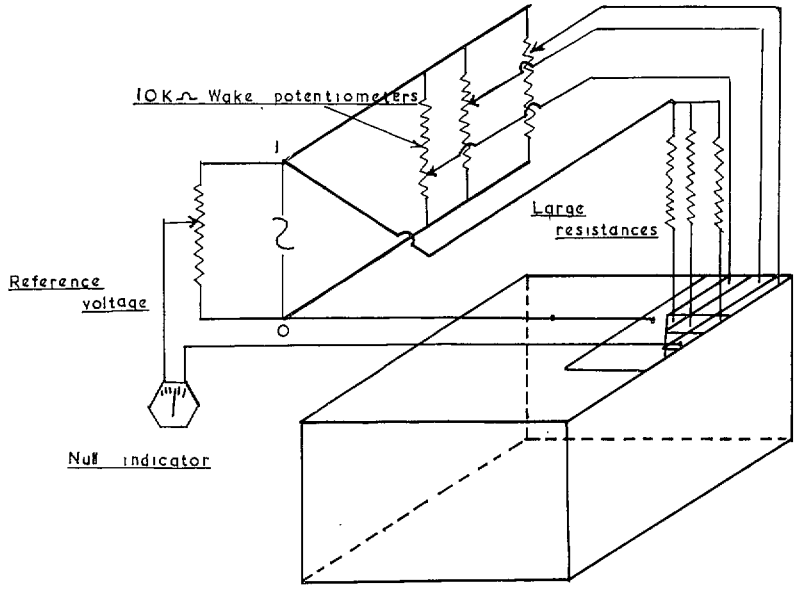

FIG. 4. The direct-analogy circuit.

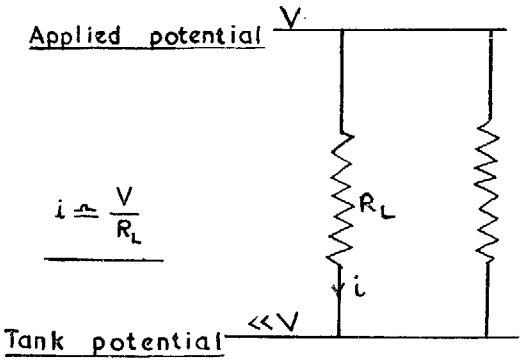

FIG. 5. Behaviour of large resistances.

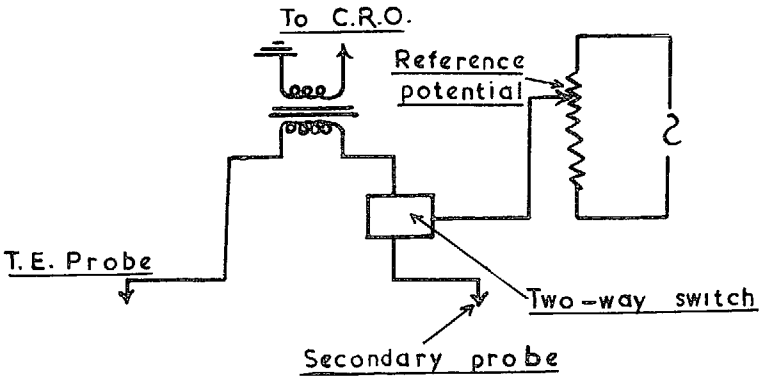

FIG. 6. Kutta-Joukowsky balance circuit.

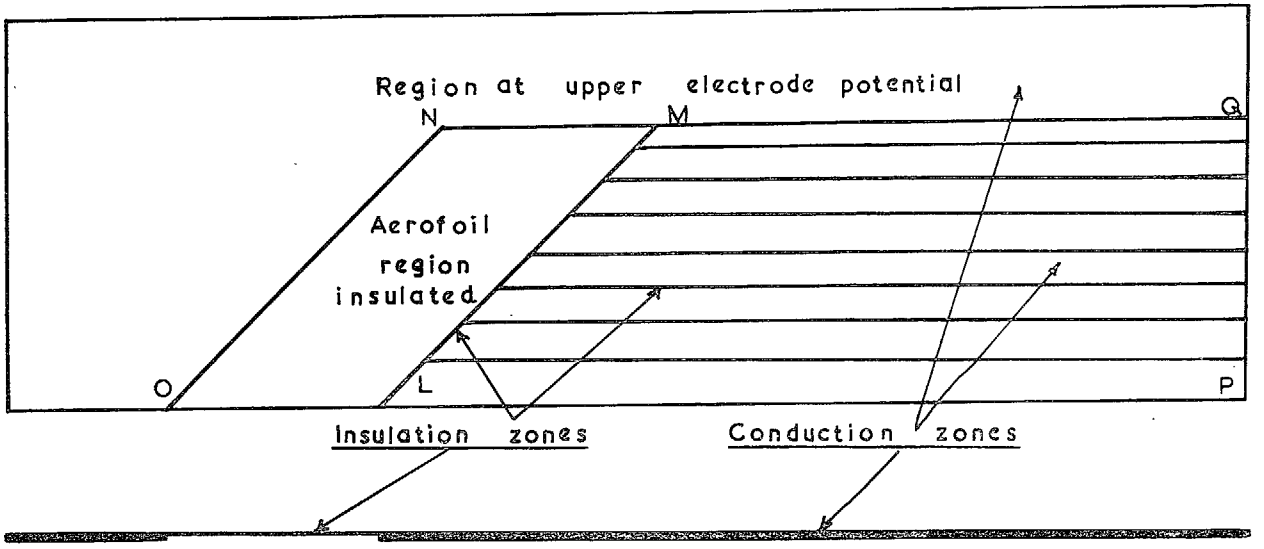

FIG. 7. The transverse-analogy model.

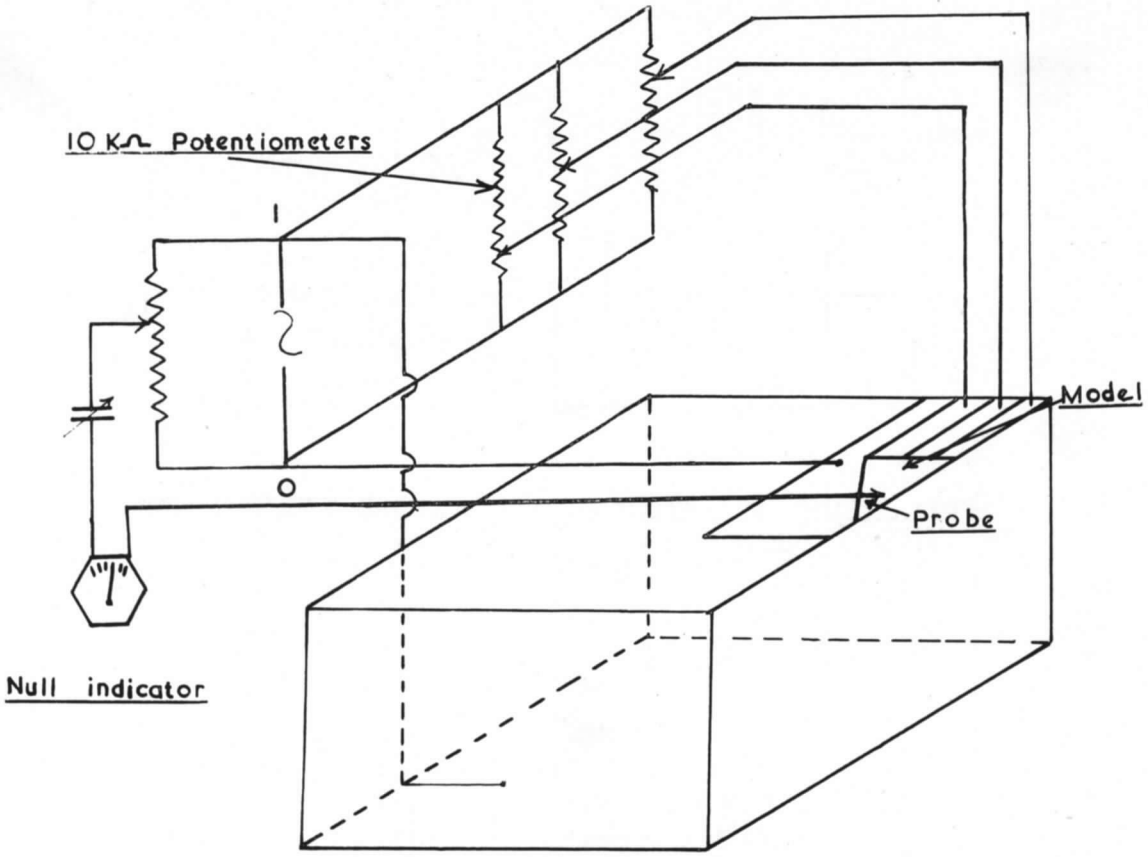

FIG. 8. The transverse-analogy circuit.

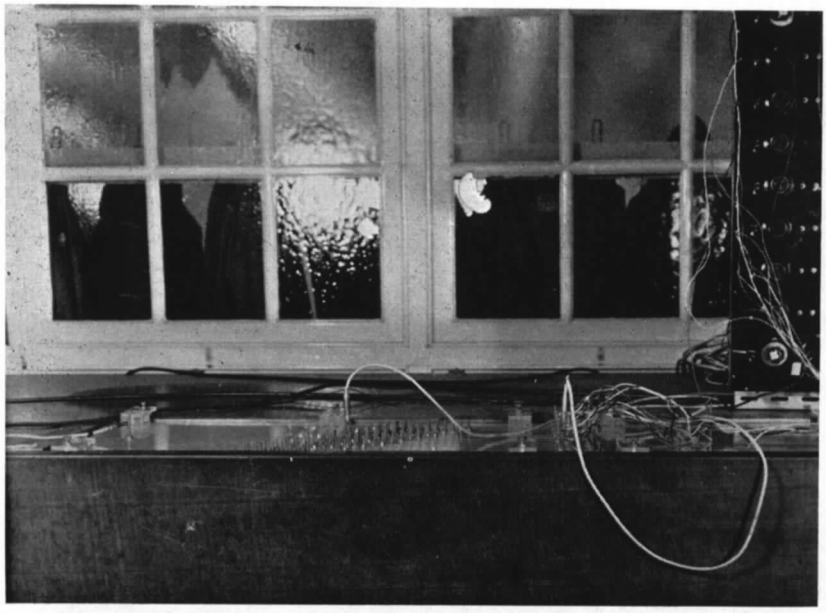

FIG. 9. Model placed in upper-electrode cut.

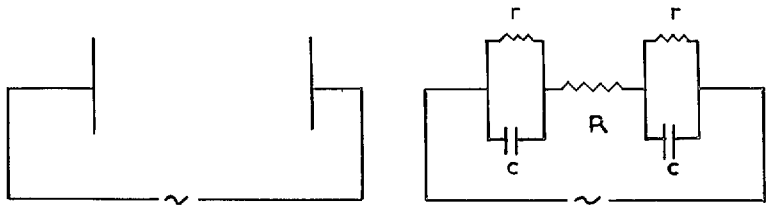

Cross section of electrolytic tank.

Equivalent electric circuit.

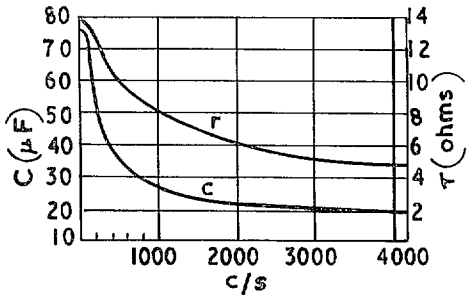

Electrode surface components of polished Cu electrodes and a 0·5 M $Cu\,So_4$ solution. (After Einstein).

FIG. 10. Electrode surface impedance.

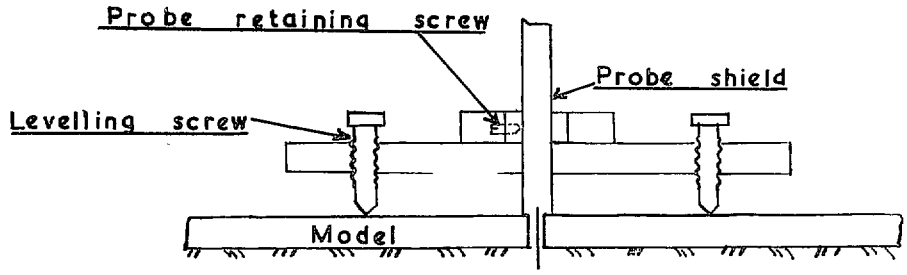

FIG. 11. Probe holder.

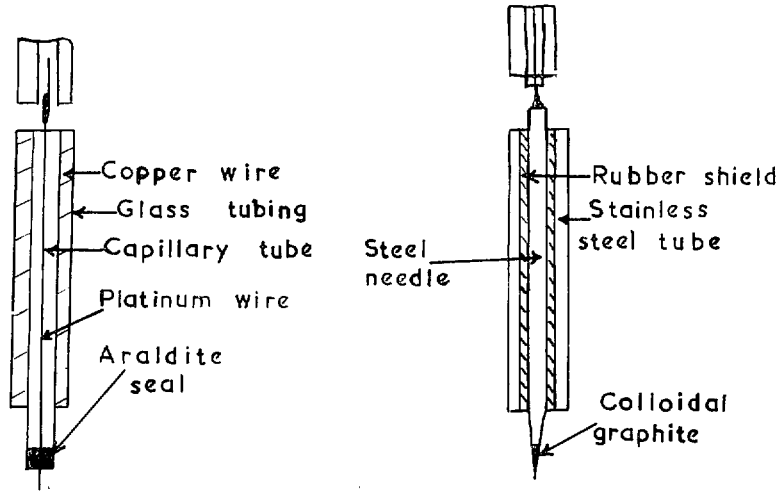

FIG. 12. Details of the probes.

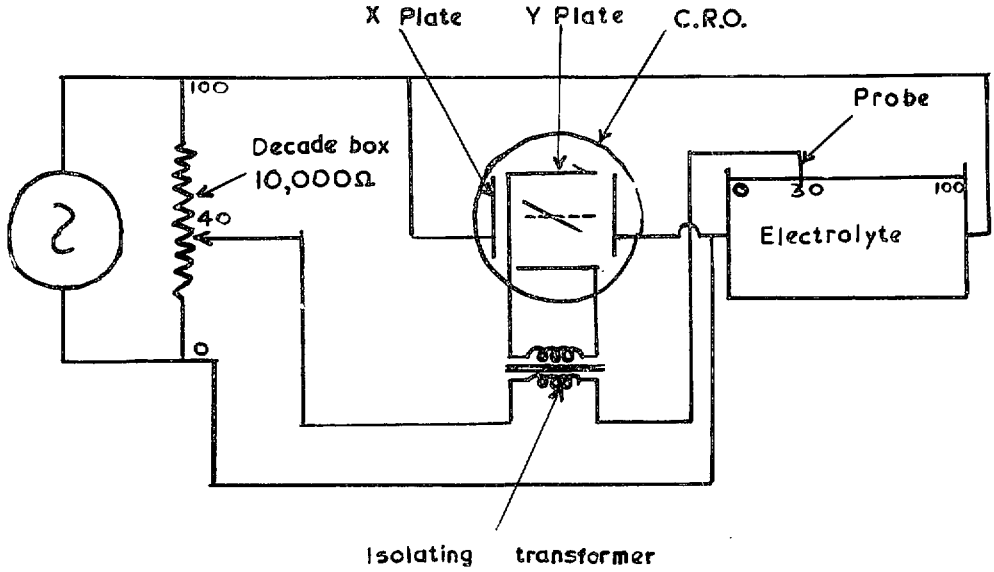

FIG. 13. Potential measuring circuit.

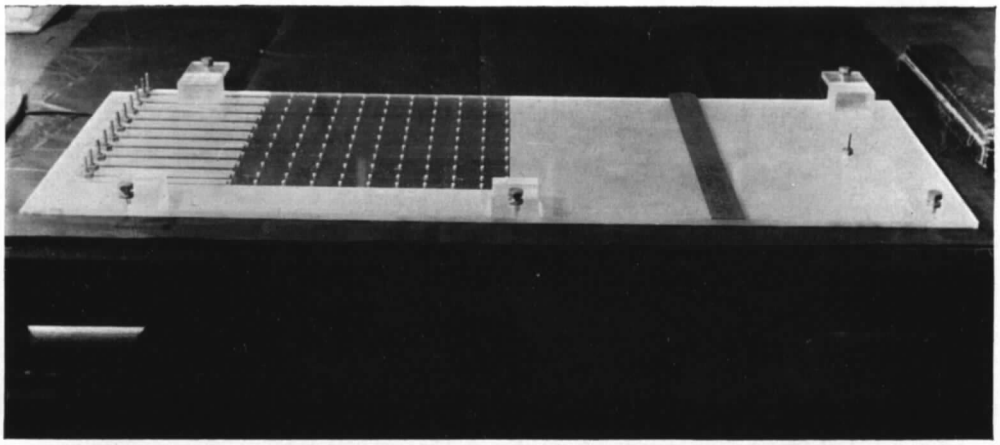

FIG. 14. Model of rectangular wing.

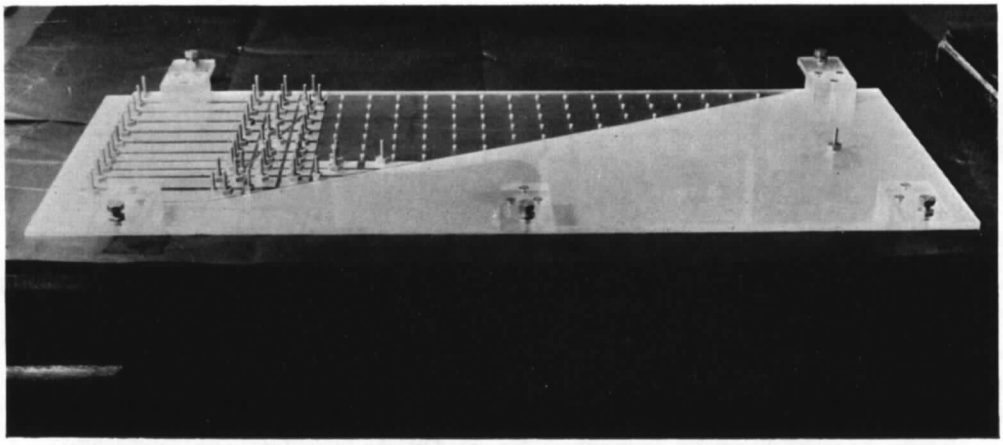

FIG. 15. Model of delta wing.

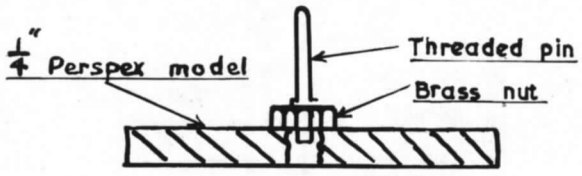

FIG. 16. Model electrode.

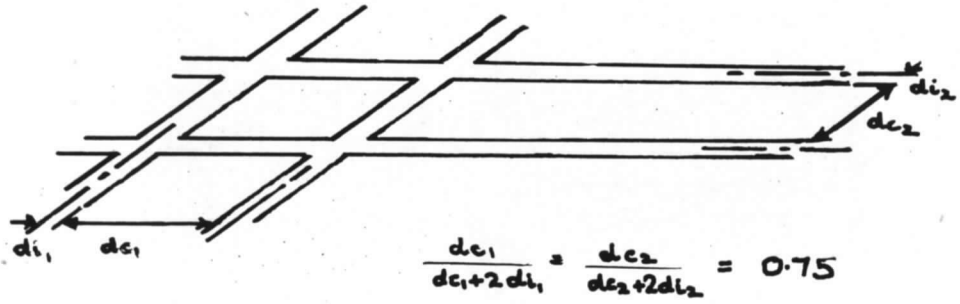

FIG. 17. Recommended model electrode dimensions.

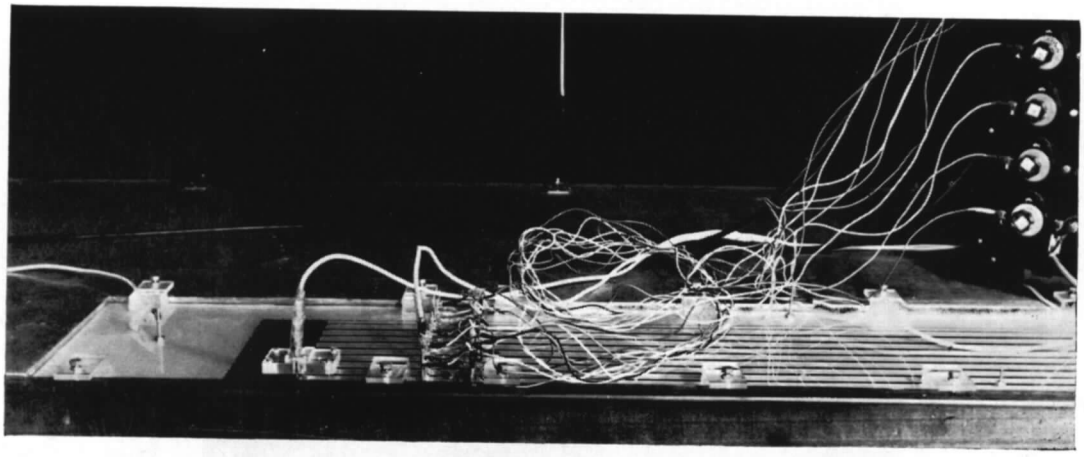

FIG. 18. Connection of two halves of model.

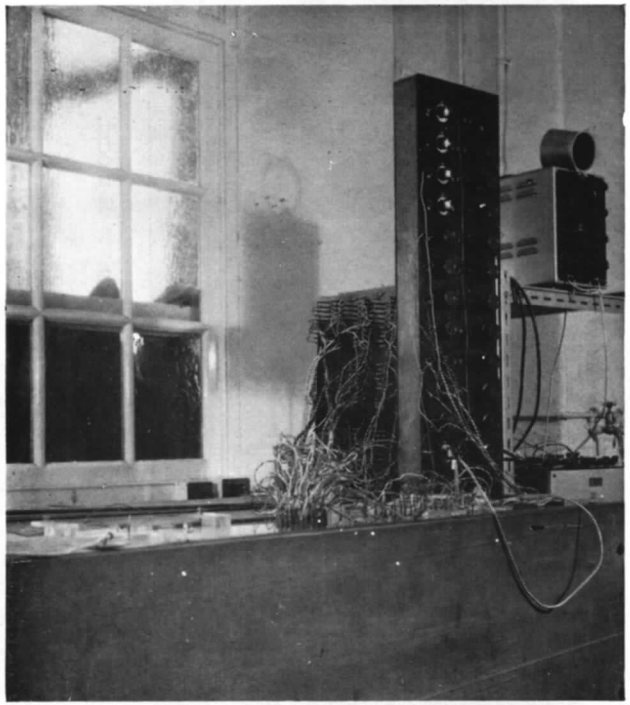

FIG. 19. The auxiliary network.

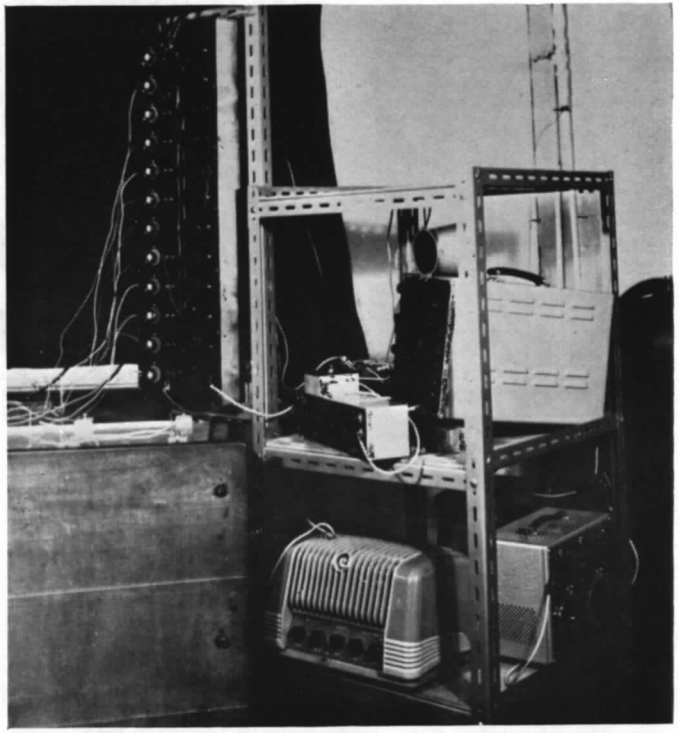

FIG. 20. The power supply and detector.

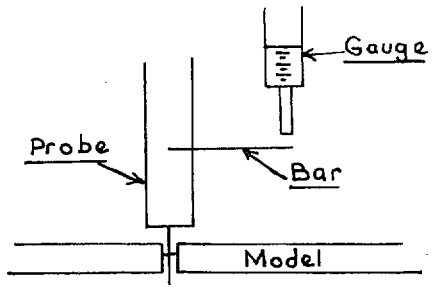

FIG. 21. Measurement of probe depth.

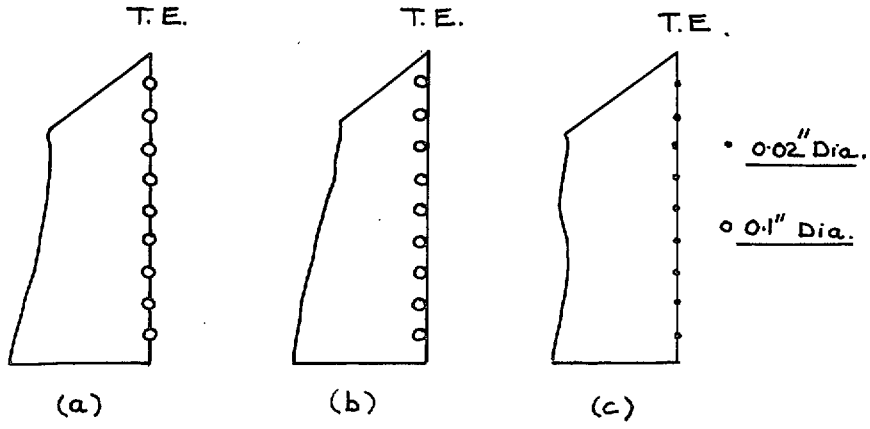

FIG. 22. Three trailing-edge configurations.

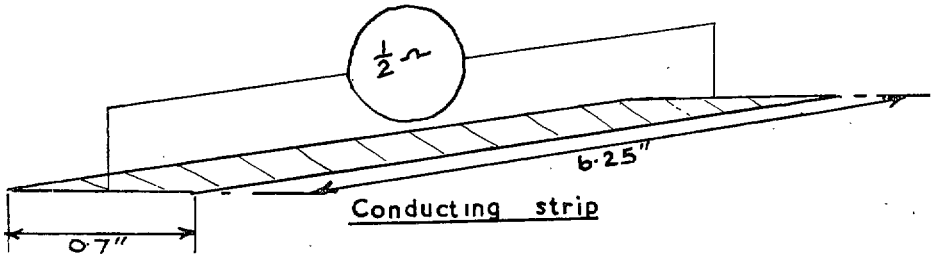

FIG. 23. Resistivity of silver-painted surface.

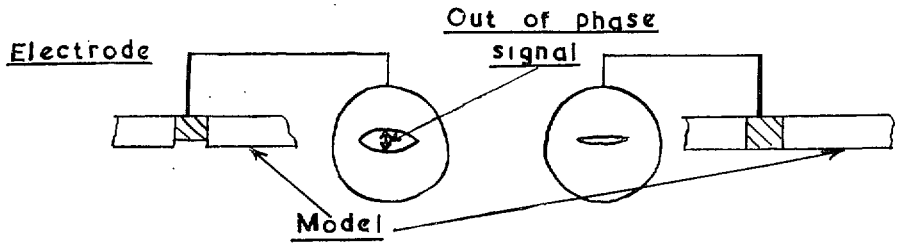

FIG. 24. Reactance component of poorly fitted electrode.

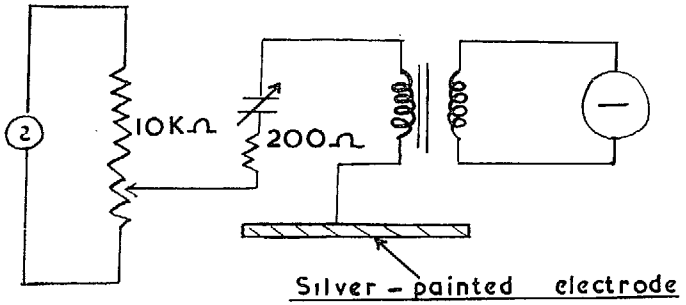

FIG. 25. Indication of capacity component.

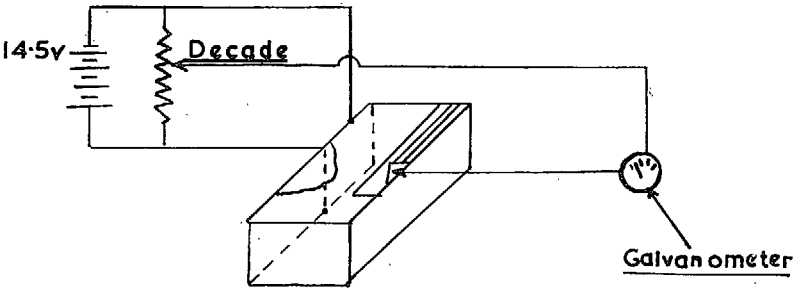

FIG. 26. D.C. circuit test.

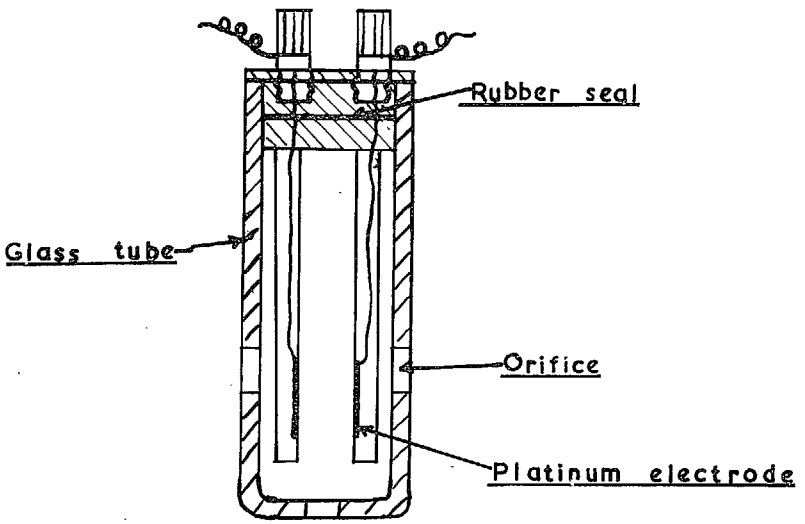

FIG. 27. Conductivity cell.

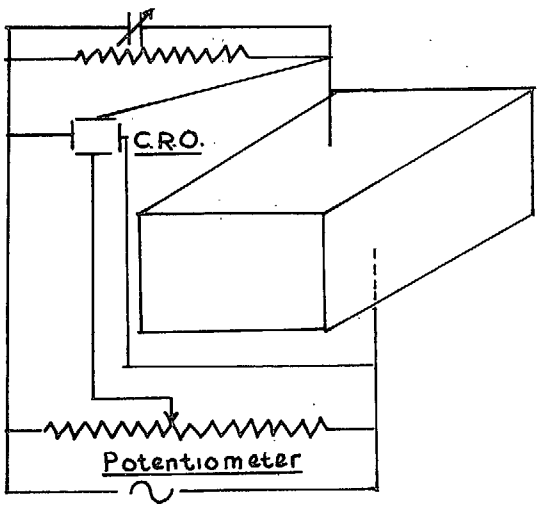

FIG. 28. Electrolyte conductivity measurement.

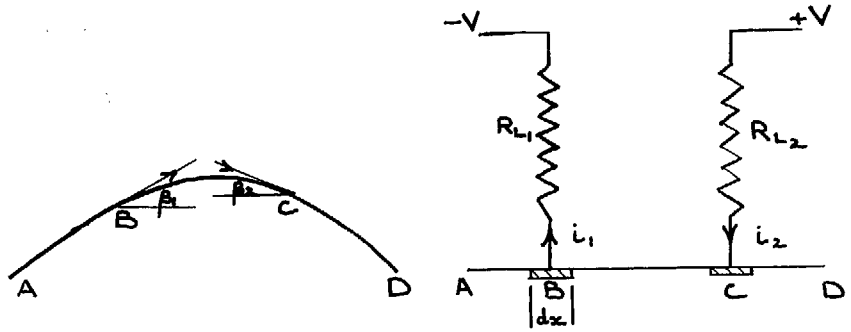

a) TANGENTIAL FLOW ON AEROFOIL.

b) ANALOGUE TANGENTIAL FLOW CONDITION.

FIGS. 29a and b.

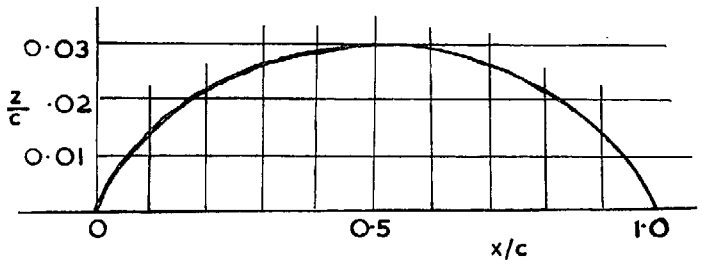

FIG. 30. Aile 1.

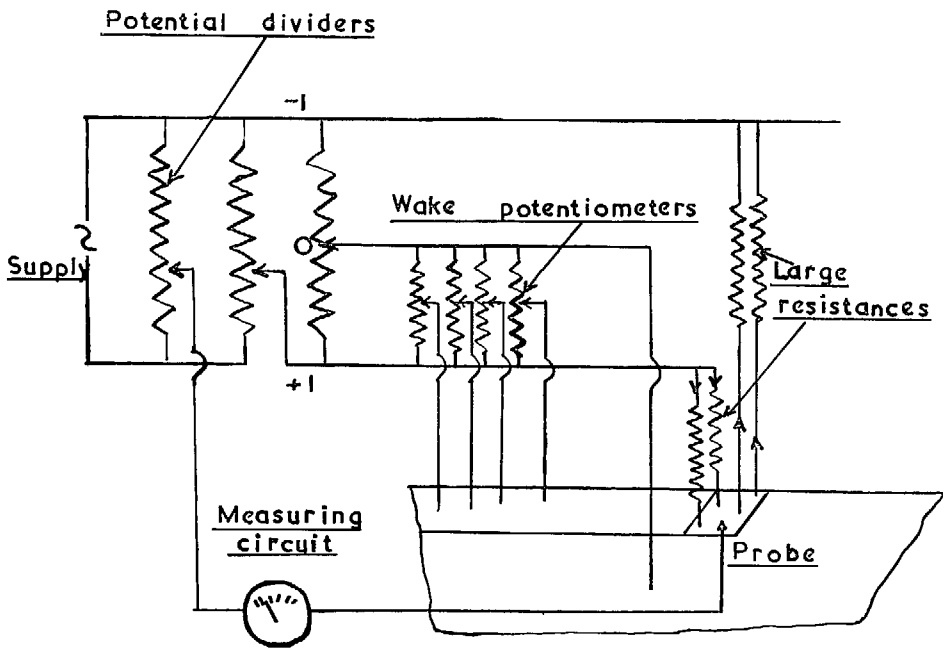

FIG. 31. Cambered-wing circuit.

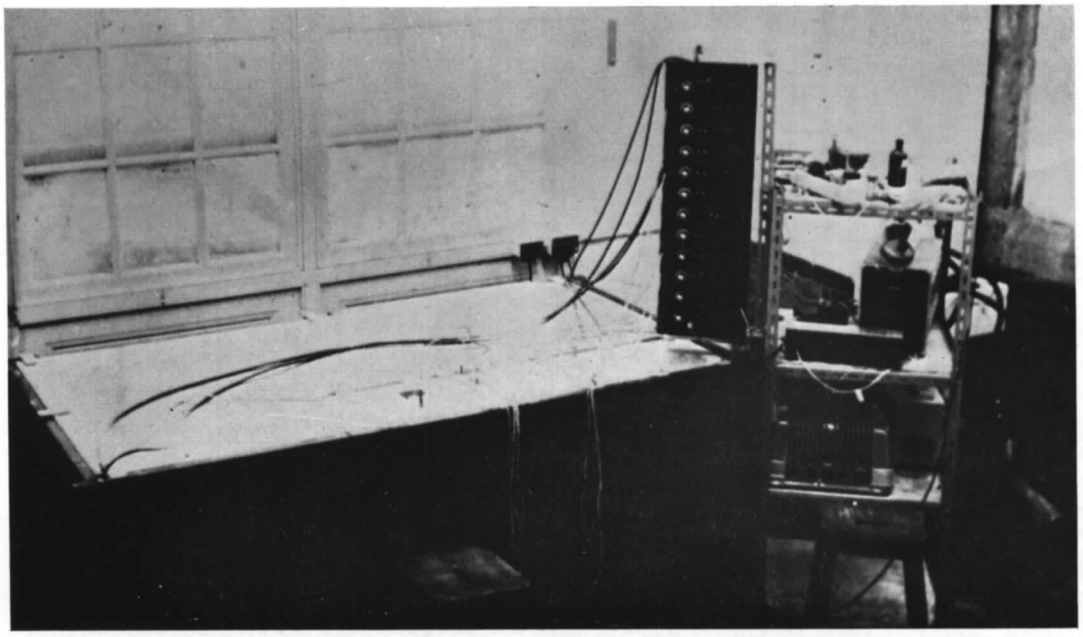

FIG. 32. General view of apparatus.

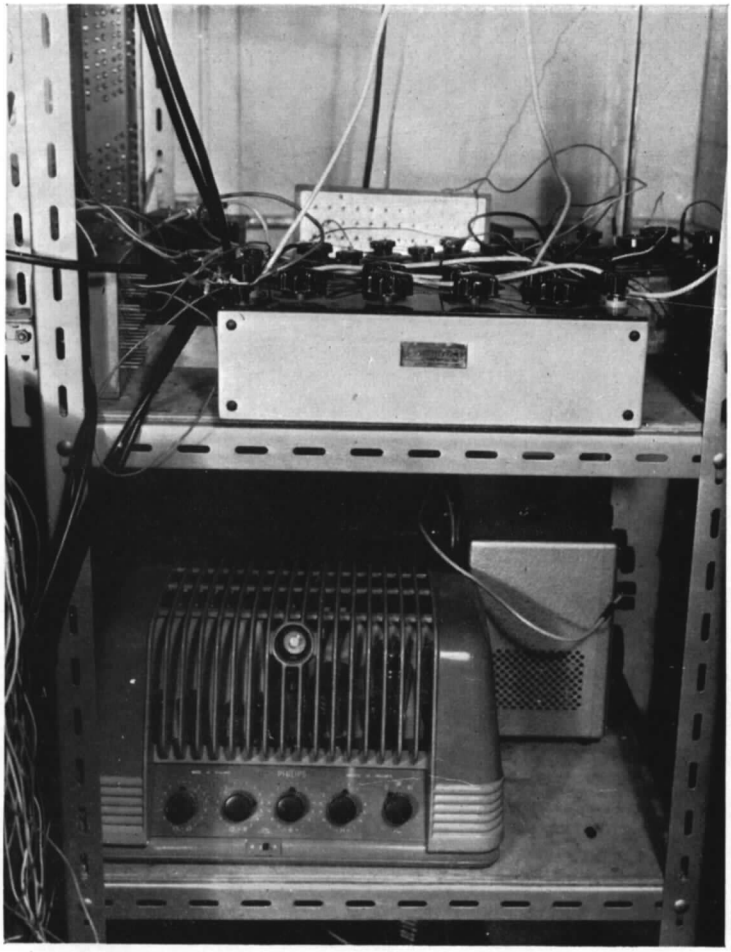

FIG. 33. The amplifier and potential divider.

(8618) Wt. 64/1857 K.5 8/63 Hw.

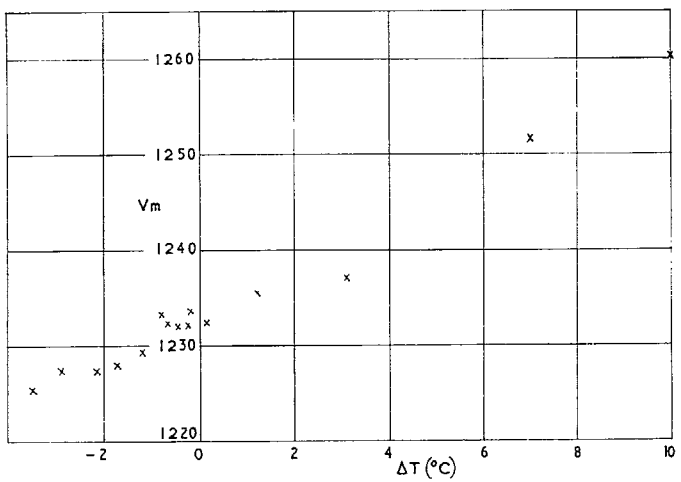

FIG. 34. ΔT results.

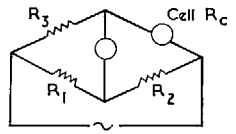

Substance in distilled water grm / 100 cc	$\sigma \times 10^4$ ohm^{-1}cm^{-1}	R_1 Ω	R_2 Ω	R_3 Ω	R_c Ω	Temp °C
KNo_3 10grm	839	9000	1000	90	10	19 °C
KNo_3 15grm	1186	9000	1000	80	9	19 °C
$CuSo_4$ 5grm	189	9000	1000	408	45	19 °C
NaCl 15grm	1642	9000	1000	69	8	19 °C
NaCl 25grm	2135	9000	1000	52	6	19 °C
KCl 5 grm	690	9000	1000	130	14	19 °C

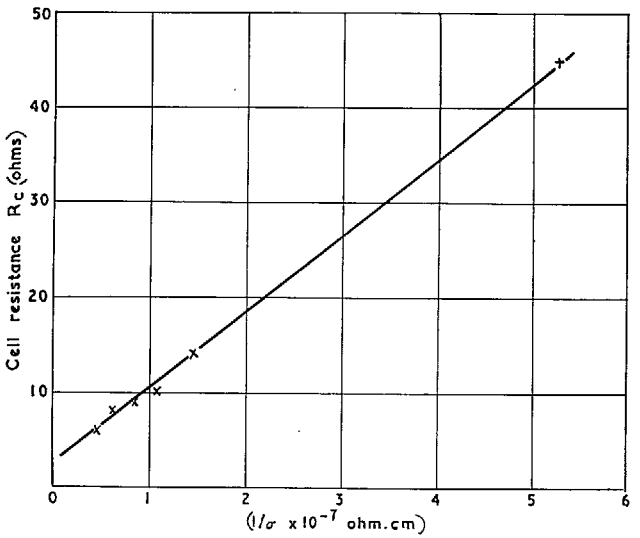

FIG. 35. Conductivity cell calibration.

Publications of the Aeronautical Research Council

ANNUAL TECHNICAL REPORTS OF THE AERONAUTICAL RESEARCH COUNCIL (BOUND VOLUMES)

1942 Vol. I. Aero and Hydrodynamics, Aerofoils, Airscrews, Engines. 75*s.* (post 2*s.* 9*d.*)
Vol. II. Noise, Parachutes, Stability and Control, Structures, Vibration, Wind Tunnels. 47*s.* 6*d.* (post 2*s.* 3*d.*)

1943 Vol. I. Aerodynamics, Aerofoils, Airscrews. 80*s.* (post 2*s.* 6*d.*)
Vol. II. Engines, Flutter, Materials, Parachutes, Performance, Stability and Control, Structures. 90*s.* (post 2*s.* 9*d.*)

1944 Vol. I. Aero and Hydrodynamics, Aerofoils, Aircraft, Airscrews, Controls. 84*s.* (post 3*s.*)
Vol. II. Flutter and Vibration, Materials, Miscellaneous, Navigation, Parachutes, Performance, Plates and Panels, Stability, Structures, Test Equipment, Wind Tunnels. 84*s.* (post 3*s.*)

1945 Vol. I. Aero and Hydrodynamics, Aerofoils. 130*s.* (post 3*s.* 6*d.*)
Vol. II. Aircraft, Airscrews, Controls. 130*s.* (post 3*s.* 6*d.*)
Vol. III. Flutter and Vibration, Instruments, Miscellaneous, Parachutes, Plates and Panels, Propulsion. 130*s.* (post 3*s.* 3*d.*)
Vol. IV. Stability, Structures, Wind Tunnels, Wind Tunnel Technique. 130*s.* (post 3*s.* 3*d.*)

1946 Vol. I. Accidents, Aerodynamics, Aerofoils and Hydrofoils. 168*s.* (post 3*s.* 9*d.*)
Vol. II. Airscrews, Cabin Cooling, Chemical Hazards, Controls, Flames, Flutter, Helicopters, Instruments and Instrumentation, Interference, Jets, Miscellaneous, Parachutes. 168*s.* (post 3*s.* 3*d.*)
Vol. III. Performance, Propulsion, Seaplanes, Stability, Structures, Wind Tunnels. 168*s.* (post 3*s.* 6*d.*)

1947 Vol. I. Aerodynamics, Aerofoils, Aircraft. 168*s.* (post 3*s.* 9*d.*)
Vol. II. Airscrews and Rotors, Controls, Flutter, Materials, Miscellaneous, Parachutes, Propulsion, Seaplanes, Stability, Structures, Take-off and Landing. 168*s.* (post 3*s.* 9*d.*)

1948 Vol. I. Aerodynamics, Aerofoils, Aircraft, Airscrews, Controls, Flutter and Vibration, Helicopters, Instruments, Propulsion, Seaplane, Stability, Structures, Wind Tunnels. 130*s.* (post 3*s.* 3*d.*)
Vol. II. Aerodynamics, Aerofoils, Aircraft, Airscrews, Controls, Flutter and Vibration, Helicopters, Instruments, Propulsion, Seaplane, Stability, Structures, Wind Tunnels. 110*s.* (post 3*s.* 3*d.*)

Special Volumes

Vol. I. Aero and Hydrodynamics, Aerofoils, Controls, Flutter, Kites, Parachutes, Performance, Propulsion, Stability. 126*s.* (post 3*s.*)
Vol. II. Aero and Hydrodynamics, Aerofoils, Airscrews, Controls, Flutter, Materials, Miscellaneous, Parachutes, Propulsion, Stability, Structures. 147*s.* (post 3*s.*)
Vol. III. Aero and Hydrodynamics, Aerofoils, Airscrews, Controls, Flutter, Kites, Miscellaneous, Parachutes, Propulsion, Seaplanes, Stability, Structures, Test Equipment. 189*s.* (post 3*s.* 9*d.*)

Reviews of the Aeronautical Research Council

1939–48 3*s.* (post 6*d.*) 1949–54 5*s.* (post 5*d.*)

Index to all Reports and Memoranda published in the Annual Technical Reports

1909–1947 R. & M. 2600 (out of print)

Indexes to the Reports and Memoranda of the Aeronautical Research Council

Between Nos. 2351–2449	R. & M. No. 2450 2*s.* (post 3*d.*)
Between Nos. 2451–2549	R. & M. No. 2550 2*s.* 6*d.* (post 3*d.*)
Between Nos. 2551–2649	R. & M. No. 2650 2*s.* 6*d.* (post 3*d.*)
Between Nos. 2651–2749	R. & M. No. 2750 2*s.* 6*d.* (post 3*d.*)
Between Nos. 2751–2849	R. & M. No. 2850 2*s.* 6*d.* (post 3*d.*)
Between Nos. 2851–2949	R. & M. No. 2950 3*s.* (post 3*d.*)
Between Nos. 2951–3049	R. & M. No. 3050 3*s.* 6*d.* (post 3*d.*)
Between Nos. 3051–3149	R. & M. No. 3150 3*s.* 6*d.* (post 3*d.*)

HER MAJESTY'S STATIONERY OFFICE

from the addresses overleaf

Printed and published by
HER MAJESTY'S STATIONERY OFFICE

To be purchased from
York House, Kingsway, London W.C.2
423 Oxford Street, London W.1
13A Castle Street, Edinburgh 2
109 St. Mary Street, Cardiff
39 King Street, Manchester 2
50 Fairfax Street, Bristol 1
35 Smallbrook, Ringway, Birmingham 5
80 Chichester Street, Belfast 1
or through any bookseller

Printed in England

S.O. Code No. 23-3301